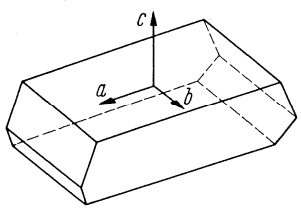

Fig. 28A-1-001. $NaNO_2$. Crystal form grown from solution [61Nom2].

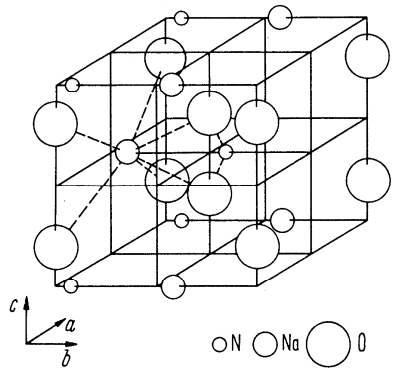

Fig. 28A-1-002. $NaNO_2$. Structure of phase III [31Zie].

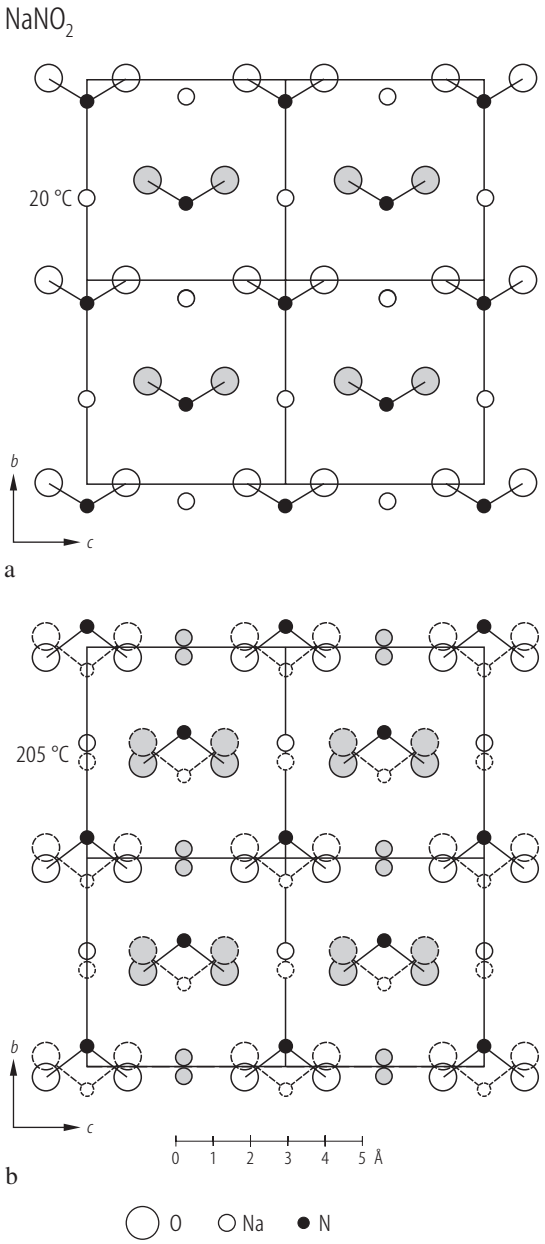

Fig. 28A-1-003. $NaNO_2$. Crystal structures. Projection along the *a* axis. (**a**) Structure of phase III [64Can], (**b**) structure of phase I [43Str]. The two positions of atoms in (**b**) are indicated by solid and dotted circles. Clear circles represent atoms placed at $x = 0$ and shaded circles those at $x = a/2$.

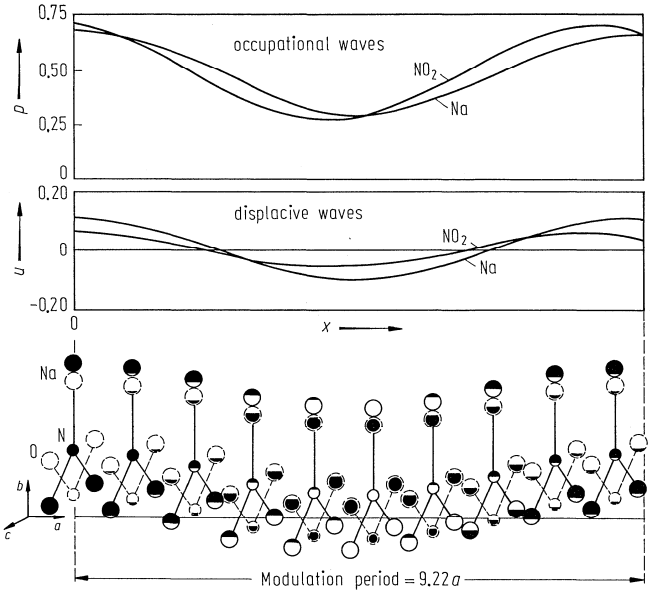

Fig. 28A-1-004. $NaNO_2$. Structure of phase II. Modulation waves for Na^+ and NO_2^- over one period of long period modulation along the *a* axis together with schematic picture of structure [85Kuc]. $T = \Theta_{III-II} + 0.2$ K. *p*, *u*: occupation probability and displacement of atoms, respectively. Note: Displacement of atoms in figure is greatly exaggerated. Atoms drawn by dashed lines represent equivalent positions allowed by symmetry. The shadowed parts represent the occupational probability.

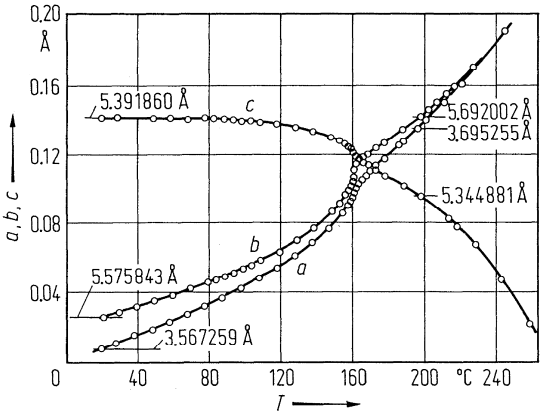

Fig. 28A-1-005. $NaNO_2$. *a*, *b*, *c* vs. *T* [76Kuc]. The ordinate indicates relative value.

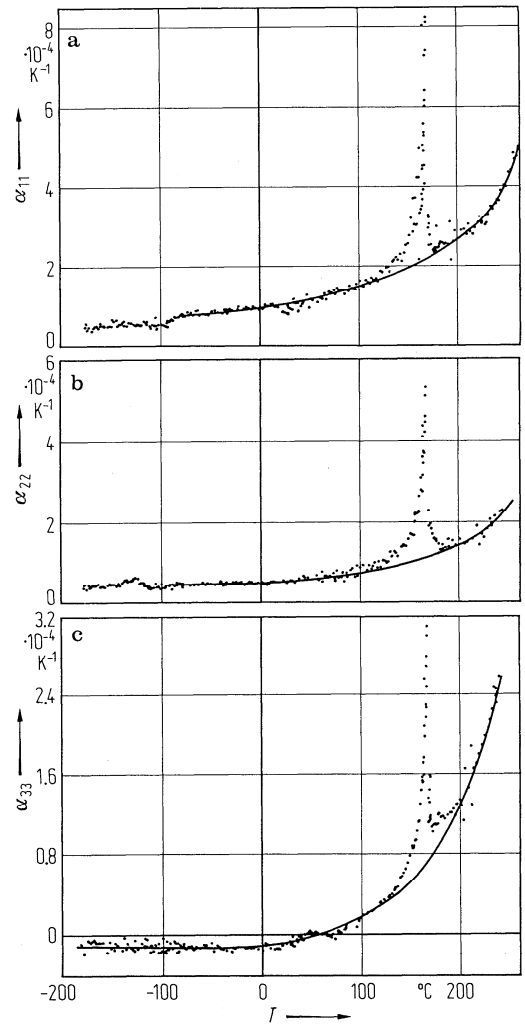

Fig. 28A-1-006. $NaNO_2$. α_{11}, α_{22}, α_{33} vs. T [75Ema]. α_{ii}: linear thermal expansion coefficient.

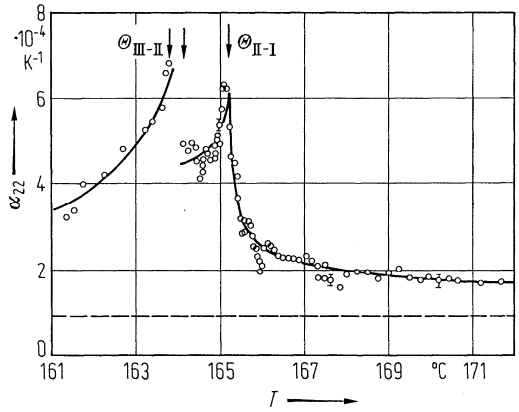

Fig. 28A-1-007. $NaNO_2$. α_{22} vs. T in the vicinity of the III–II–I transitions [75Ema].

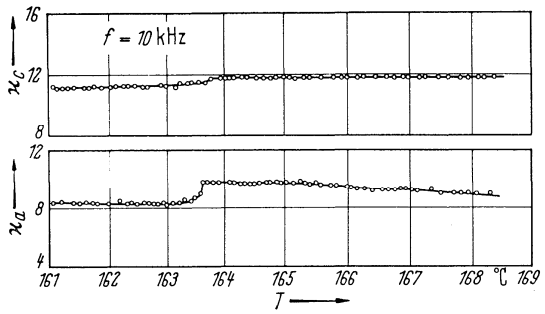

Fig. 28A-1-008. $NaNO_2$. κ_a, κ_c vs. T [67Tak].

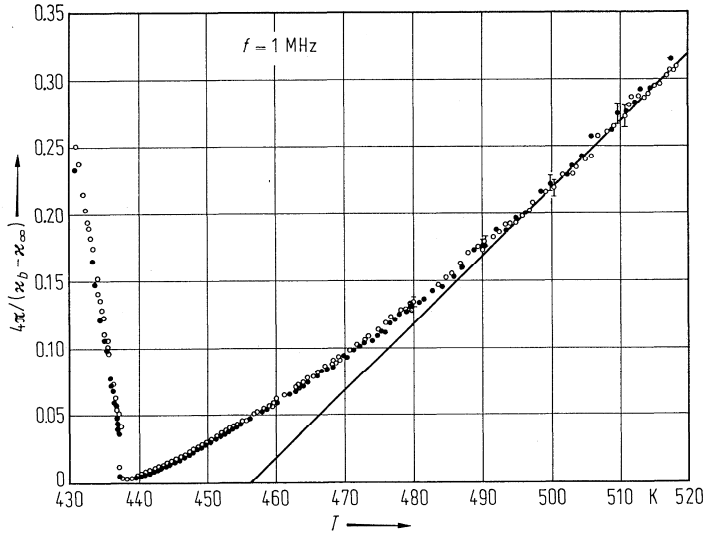

Fig. 28A-1-009. $NaNO_2$. $4\pi/(\kappa_b - \kappa_\infty)$ vs. T [75Hat]. κ_∞: dielectric constant at high frequency limit, $\kappa_\infty = 6$. Open and solid circles represent results of two different specimens, respectively.

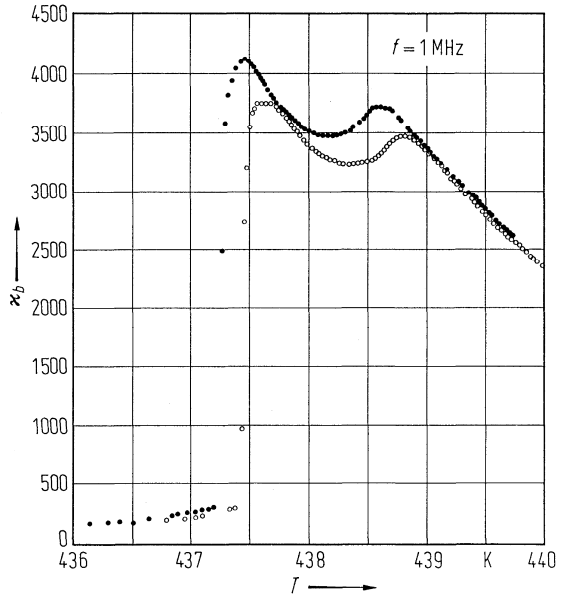

Fig. 28A-1-010. $NaNO_2$. κ_b vs. T in the vicinity of the III–II–I transitions [75Hat]. Results of two different specimens are shown by open and solid circles.

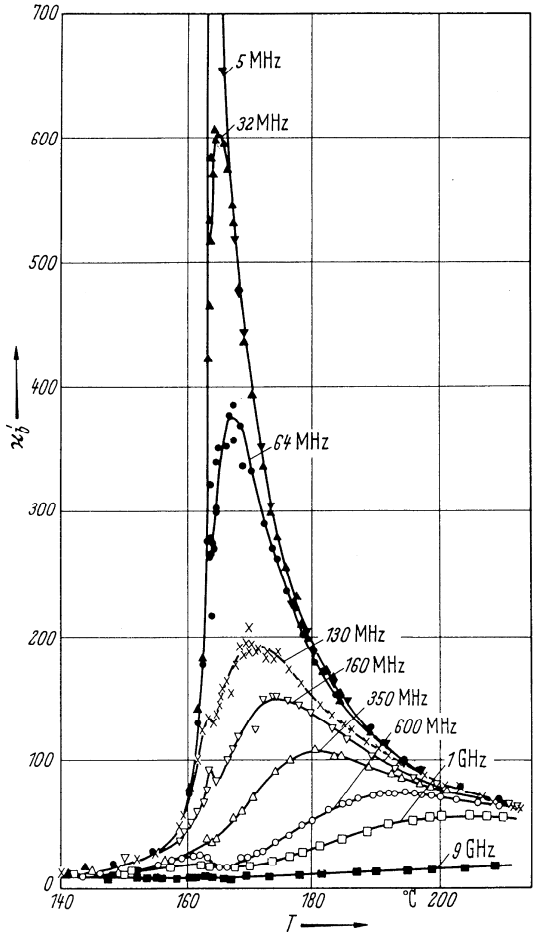

Fig. 28A-1-011. $NaNO_2$. κ_b' vs. T [68Hat]. Parameter: f.

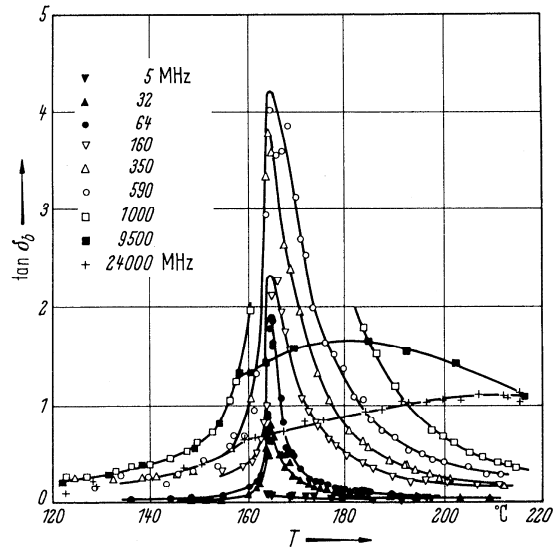

Fig. 28A-1-012. $NaNO_2$. tan δ_b vs. T [68Hat]. Parameter: f.

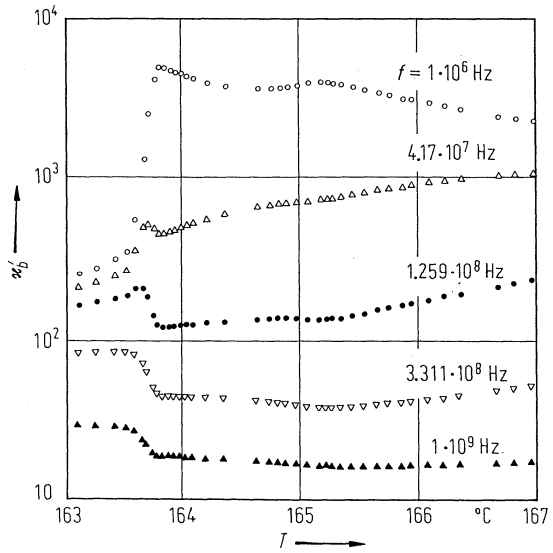

Fig. 28A-1-013. $NaNO_2$. κ_b' vs. T in the vicinity of the III–II–I transitions [86Deg]. Parameter: f.

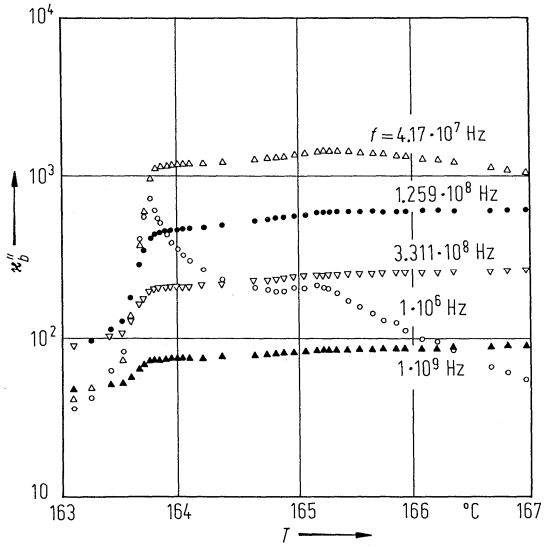

Fig. 28A-1-014. $NaNO_2$. κ_b'' vs. T in the vicinity of the III–II–I transitions [86Deg]. Parameter: f.

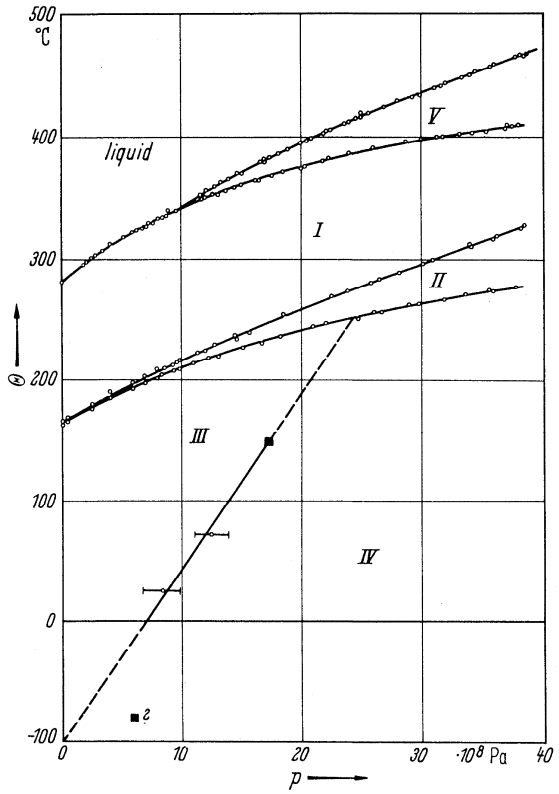

Fig. 28A-1-015. $NaNO_2$. Θ vs. p [66Rap]. The solid squares show results of [37Bri].

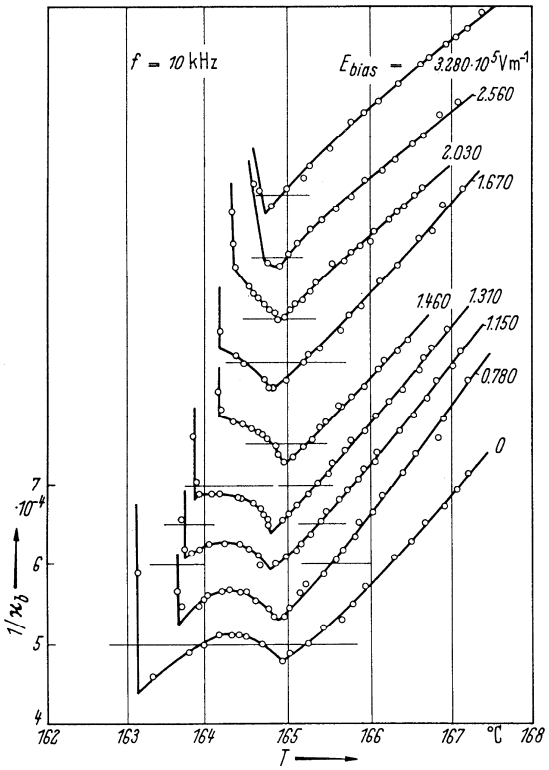

Fig. 28A-1-016. $NaNO_2$. $1/\kappa_b$ vs. T in the vicinity of the III–II–I transitions [65Ges1]. Parameter: E_{bias}. The horizontal line attaching each curve indicates the level of $1/\kappa_b = 5 \cdot 10^{-4}$.

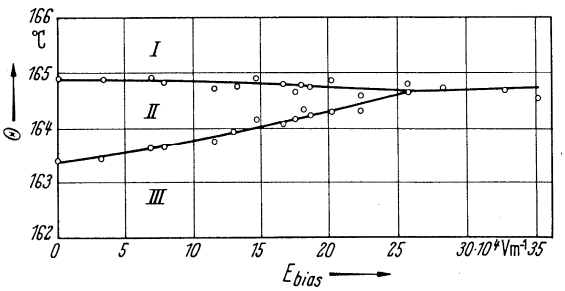

Fig. 28A-1-017. $NaNO_2$. Θ vs. E_{bias} [65Ges1].

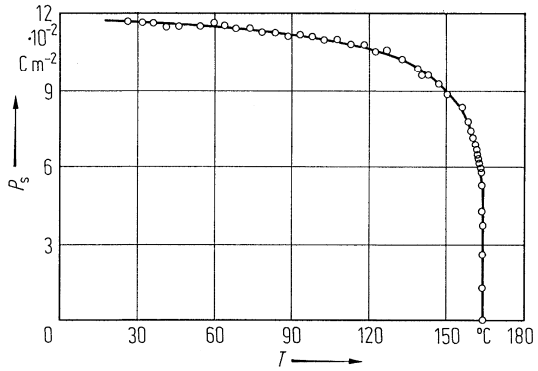

Fig. 28A-1-018. $NaNO_2$. P_s vs. T [73Ham]. Obtained from pyroelectric charge measurements.

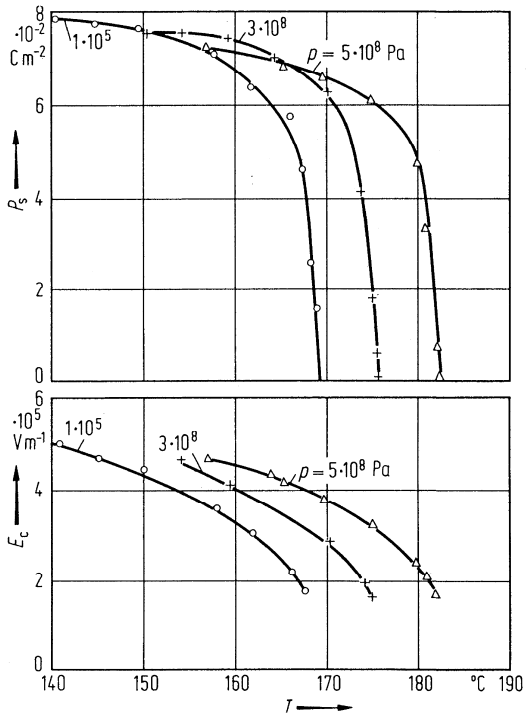

Fig. 28A-1-019. $NaNO_2$. P_s, E_c vs. T [71Leo]. Parameter: p.

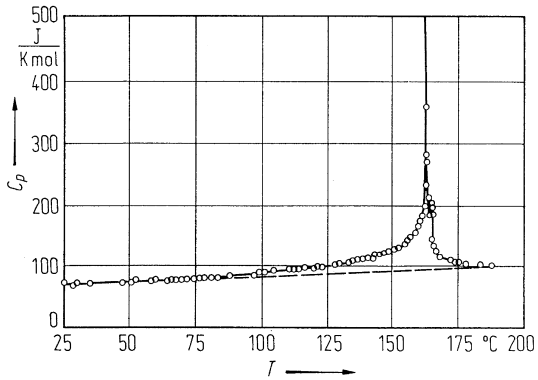

Fig. 28A-1-020. $NaNO_2$. C_p vs. T [65Sak].

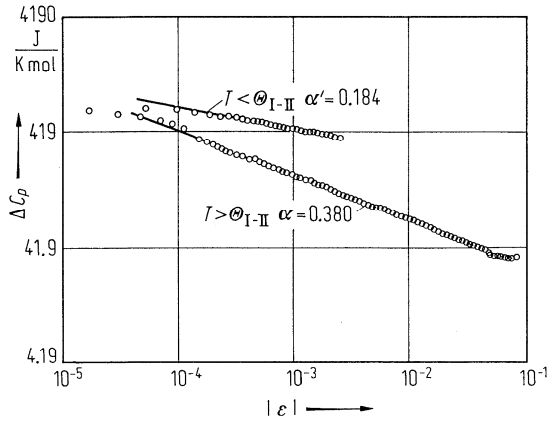

Fig. 28A-1-021. $NaNO_2$. ΔC_p vs. $|\varepsilon|$ [71Hat]. ΔC_p: excess molar heat capacity at constant pressure. $\varepsilon = (\Theta_{II-I} - T)/\Theta_{II-I}$, α, α': critical indices.

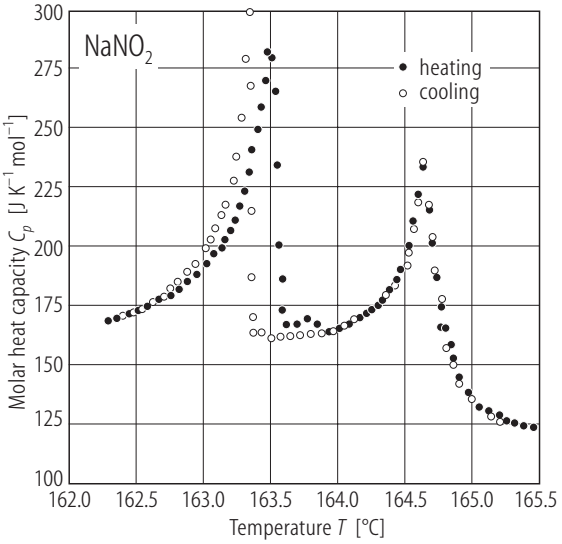

Fig. 28A-1-022. $NaNO_2$. C_p vs. T in the vicinity of the III–II–I transitions [87Yoo].

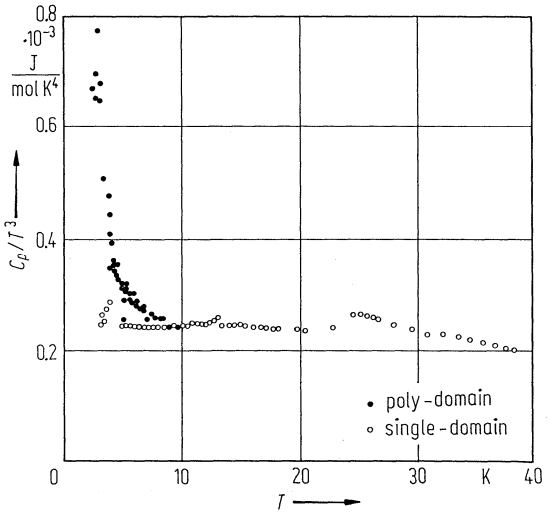

Fig. 28A-1-023. $NaNO_2$. C_p/T^3 vs. T at low temperature [81Vil]. Results for single- and poly-domain specimens are shown. C_p: molar heat capacity at constant pressure.

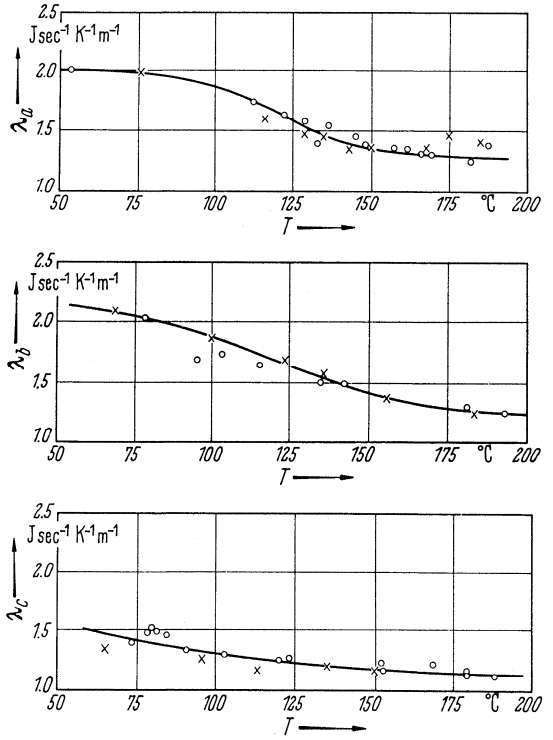

Fig. 28A-1-024. $NaNO_2$. λ_a, λ_b, λ_c vs. T [61Yos]. λ_i: thermal conductivity along the i-direction.

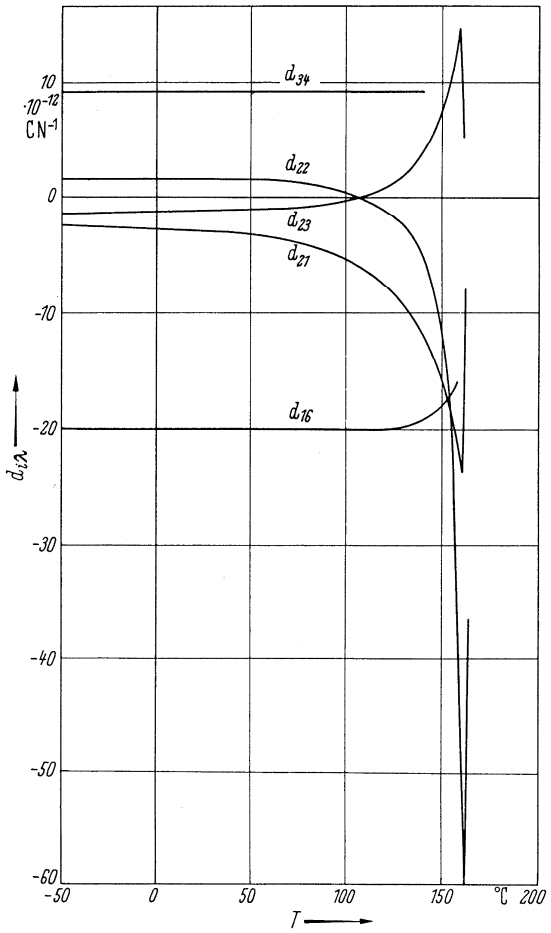

Fig. 28A-1-025. $NaNO_2$. $d_{i\lambda}$ vs. T [63Ham].

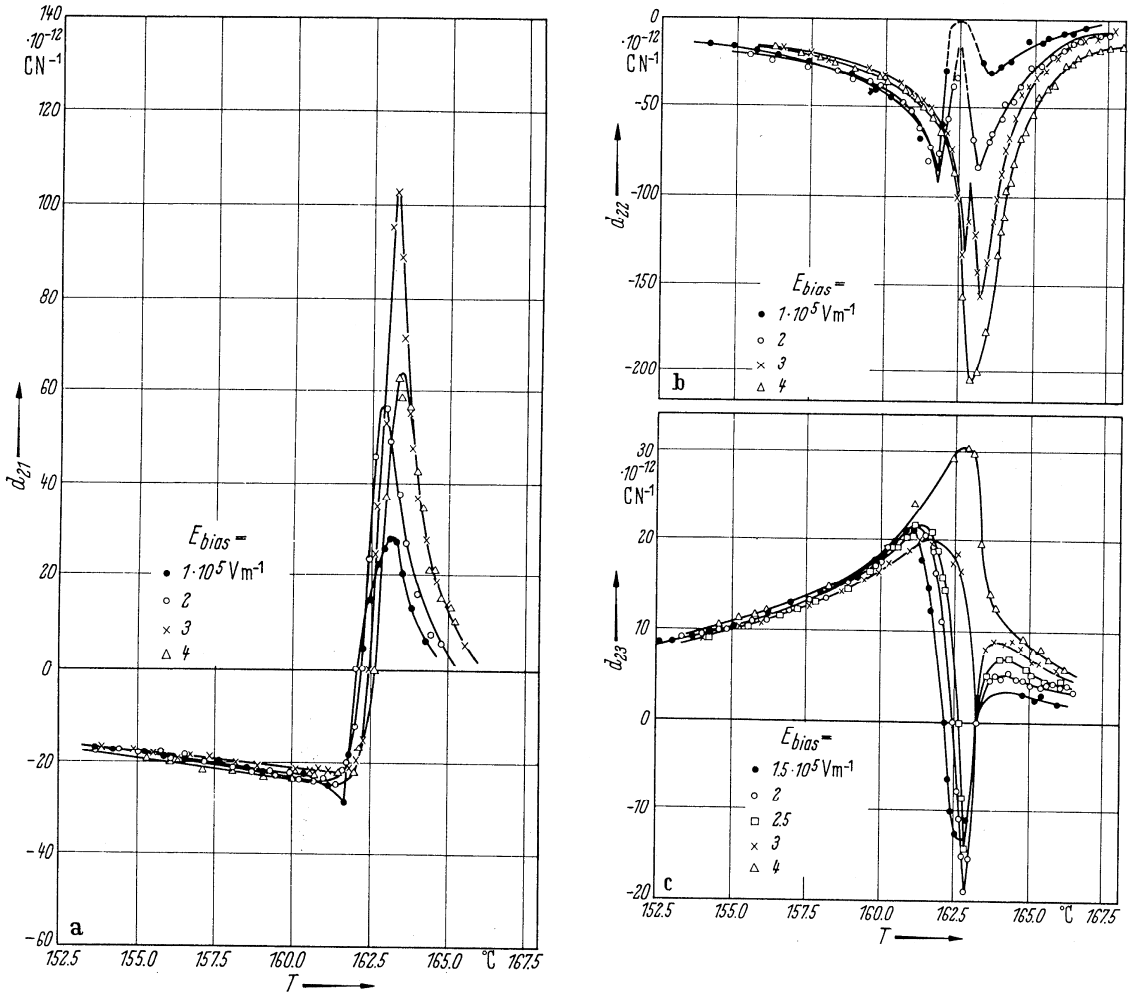

Fig. 28A-1-026. $NaNO_2$. $d_{i\lambda}$ vs. T in the vicinity of the III–II–I transitions [64Ham]. Parameter: E_{bias}. (**a**) d_{21}, (**b**) d_{22}, (**c**) d_{23}.

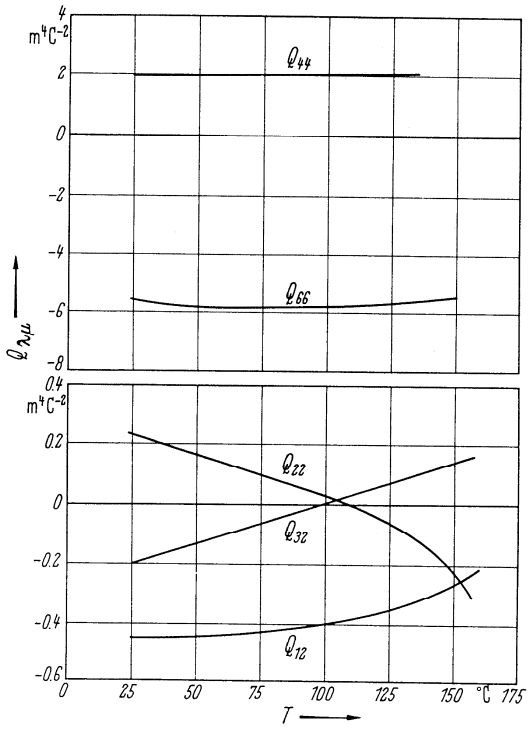

Fig. 28A-1-027. $NaNO_2$. $Q_{\lambda\mu}$ vs. T [63Ham]. Calculated from $d_{i\lambda}$, κ and P_s.

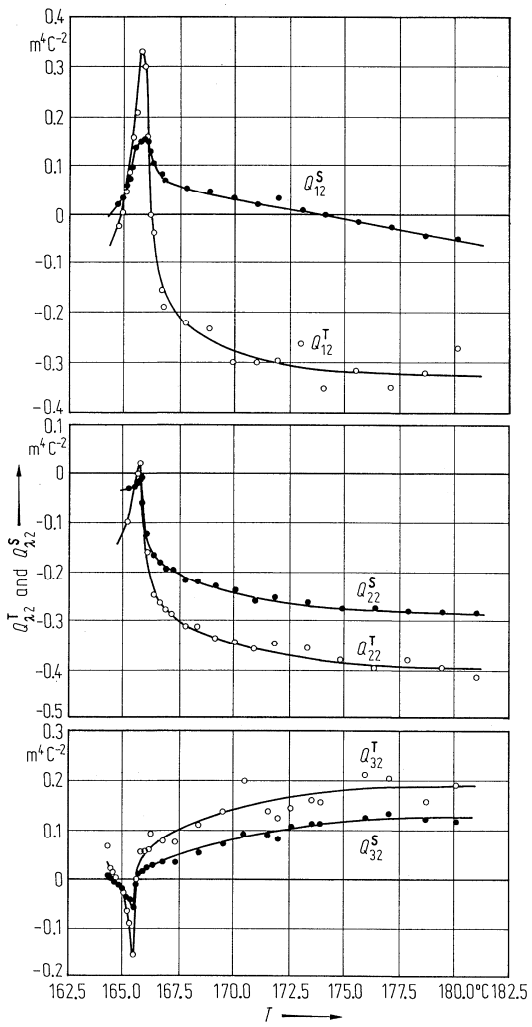

Fig. 28A-1-028. $NaNO_2$. $Q_{\lambda 2}^{\mathbf{T}}, Q_{\lambda 2}^{\mathbf{S}}$ vs. T [76Yam]. $Q_{\lambda 2}^{\mathbf{T}}, Q_{\lambda 2}^{\mathbf{S}}$: isothermal and adiabatic electrostrictive constants, respectively.

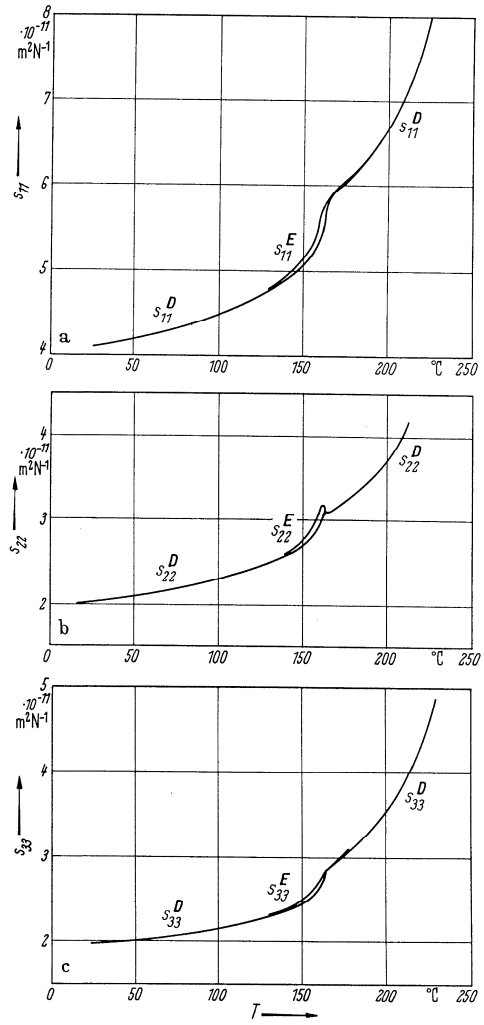

Fig. 28A-1-029. $NaNO_2$. $s_{\lambda\lambda}^{D}$, $s_{\lambda\lambda}^{E}$ vs. T [63Ham]. (**a**) $\lambda = 1$, (**b**) $\lambda = 2$, (**c**) $\lambda = 3$.

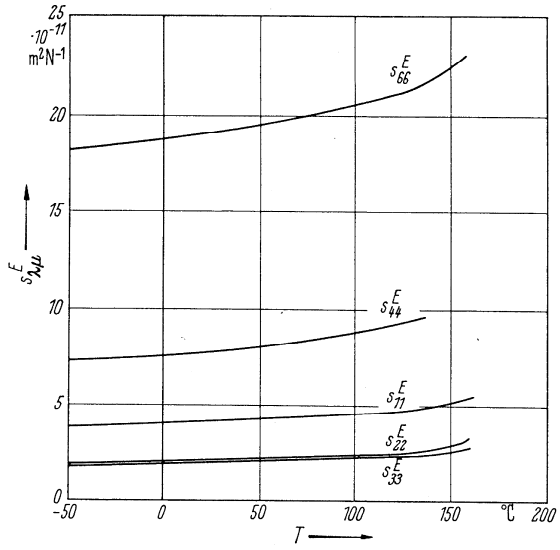

Fig. 28A-1-030. $NaNO_2$. $s^{\boldsymbol{E}}_{\lambda\mu}$ vs. T [63Ham].

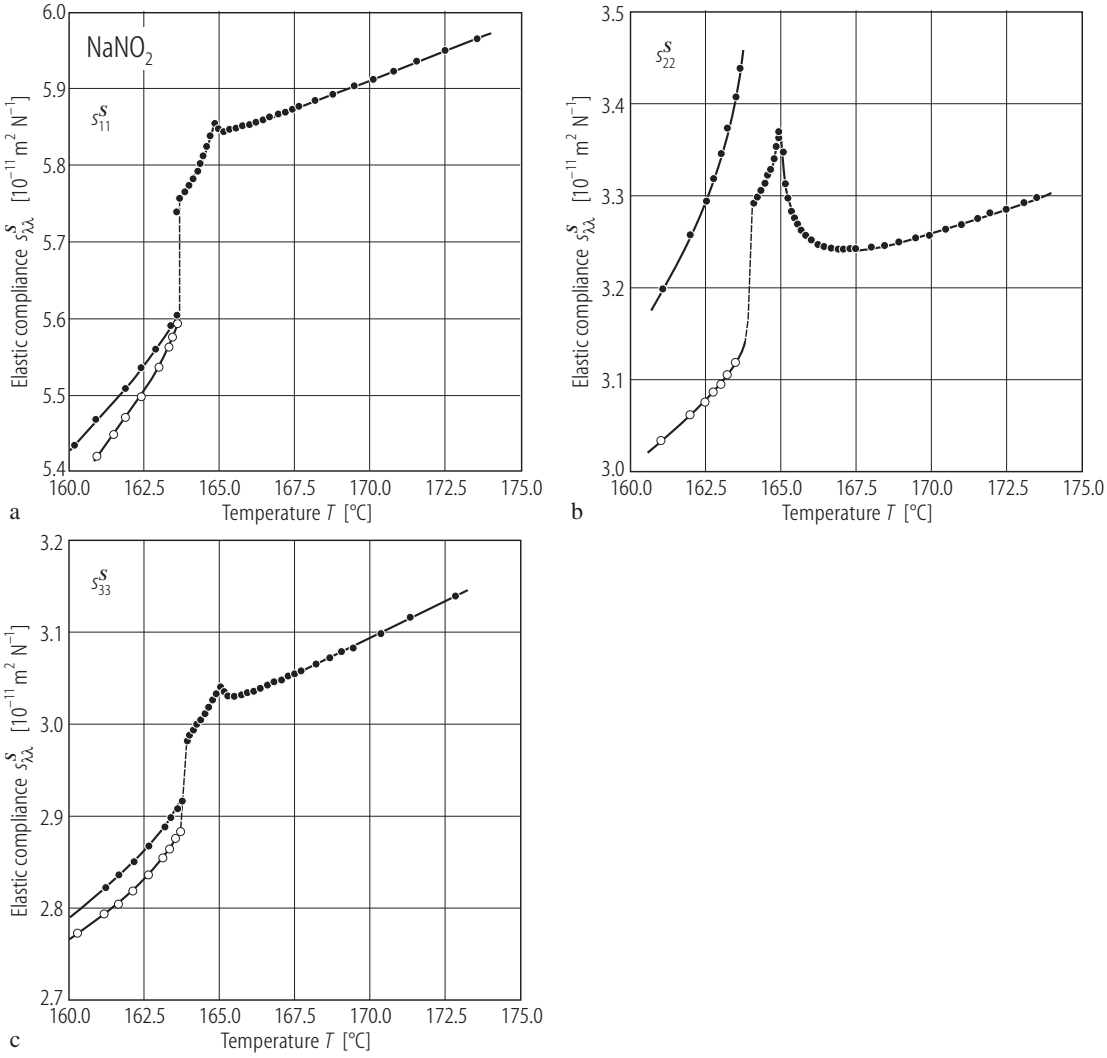

Fig. 28A-1-031. $NaNO_2$. $s^S_{\lambda\lambda}$ vs. T [78Ham]. (**a**) $\lambda = 1$, (**b**) $\lambda = 2$, (**c**) $\lambda = 3$. $s^S_{\lambda\lambda}$: adiabatic elastic compliances. In the ferroelectric phase, the elastic compliances at constant electric field, $s^{S,E}_{\lambda\lambda}$, and at constant electric displacement, $s^{S,D}_{\lambda\lambda}$, are shown by solid and open circles, respectively.

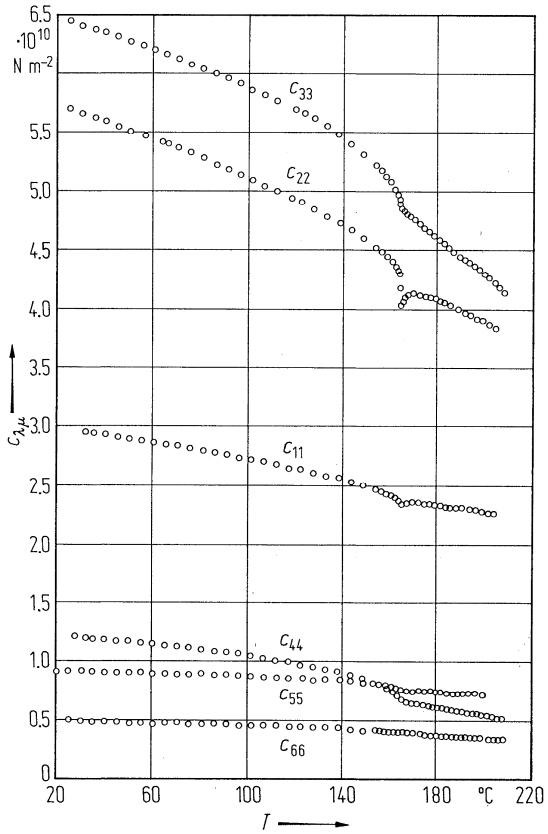

Fig. 28A-1-032. $NaNO_2$. $c_{\lambda\mu}$ vs. T [78Hat]. Obtained from ultrasonic measurements.

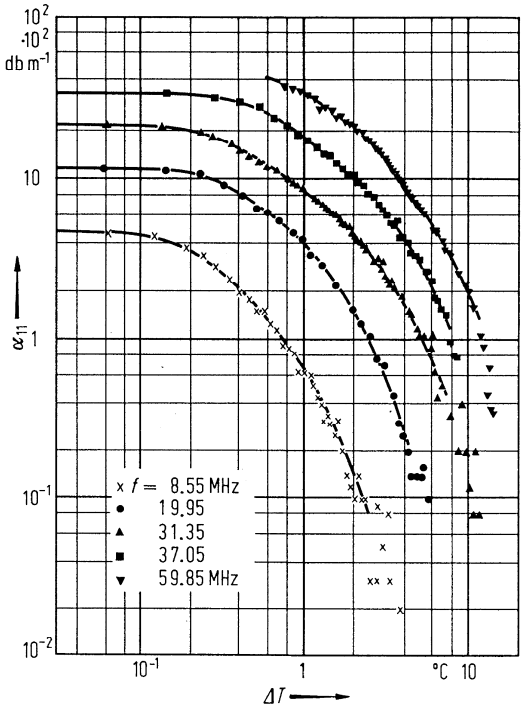

Fig. 28A-1-033. $NaNO_2$. α_{11} vs. ΔT [69Hat]. Parameter: *f*. α_{11}: attenuation coefficient of longitudinal ultrasonic waves propagating along the *a* direction. $\Delta T = T - \Theta_{II-I}$.

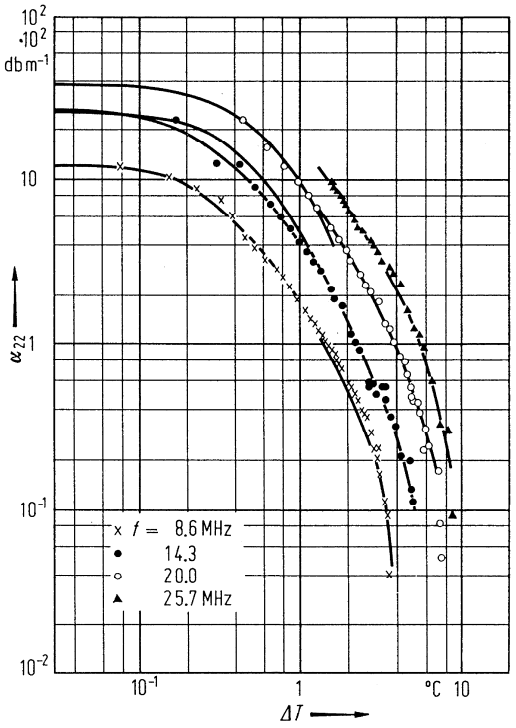

Fig. 28A-1-034. $NaNO_2$. α_{22} vs. ΔT [69Hat]. Parameter: *f*. α_{22}: attenuation coefficient of longitudinal ultrasonic waves propagating along the *b* direction. $\Delta T = T - \Theta_{II-I}$.

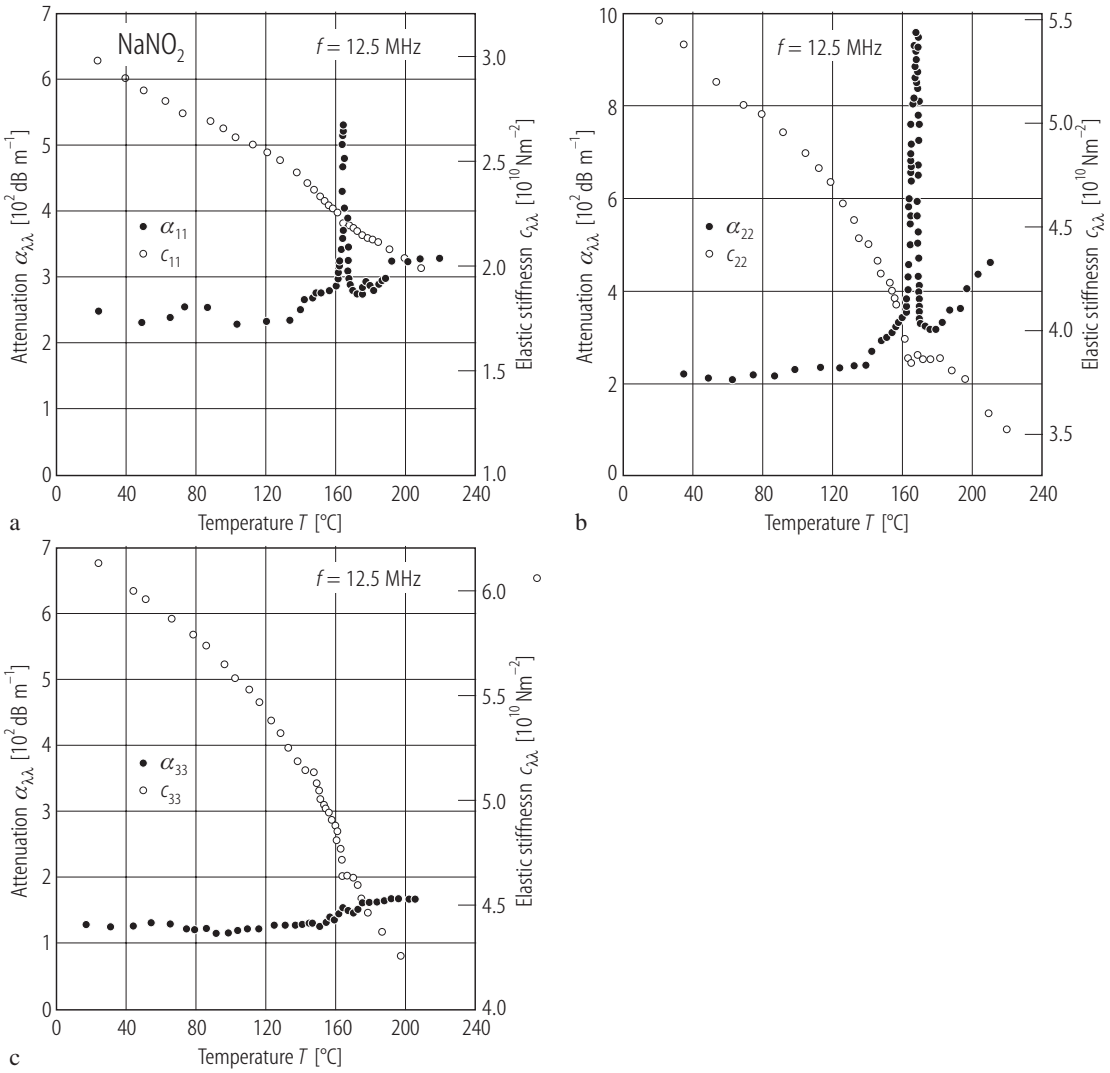

Fig. 28A-1-035. $NaNO_2$. $\alpha_{\lambda\lambda}$, $c_{\lambda\lambda}$ vs. T [70Ota]. $\alpha_{\lambda\lambda}$: attenuation coefficient of longitudinal ultrasonic wave propagating (**a**) along the *a* direction, (**b**) along the *b* direction, (**c**) along the *c* direction.

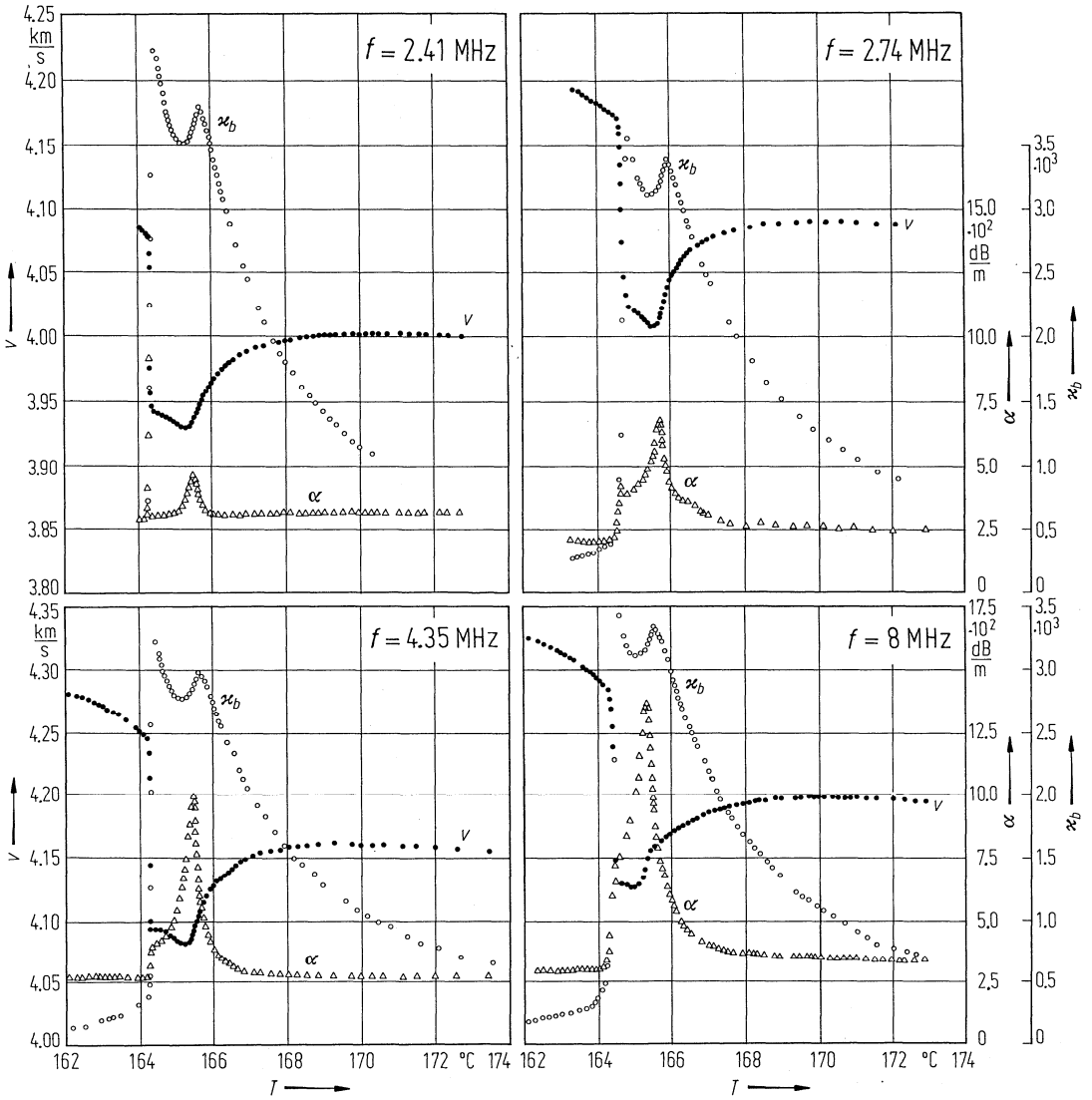

Fig. 28A-1-036. $NaNO_2$. v, α, $\varkappa_b$ vs. T [80Hat]. Parameter: f. v, α: velocity and attenuation coefficient of longitudinal sound wave propagating along the b direction, respectively. $\varkappa_b$: low frequency dielectric constant along the b direction.

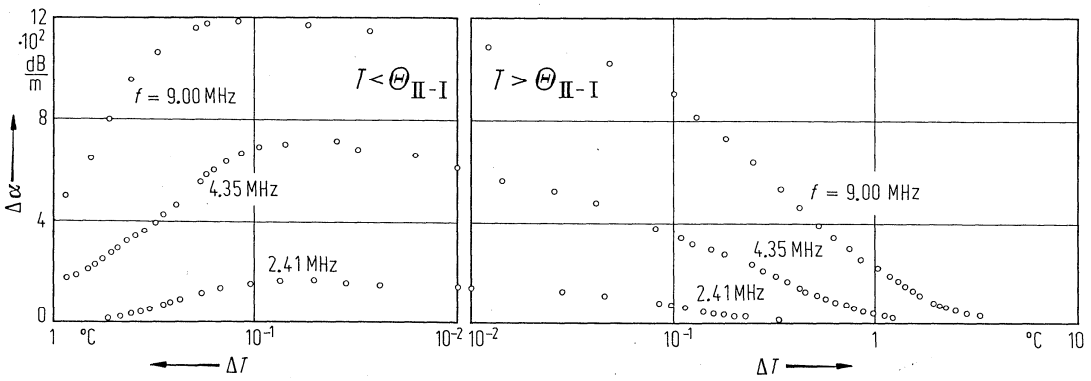

Fig. 28A-1-037. $NaNO_2$. $\Delta\alpha$ vs. ΔT [80Hat]. Parameter: f. $\Delta\alpha$: anomalous part of attenuation coefficient of longitudinal sound wave propagating along the b direction. $\Delta T = |T - \Theta_{II-I}|$.

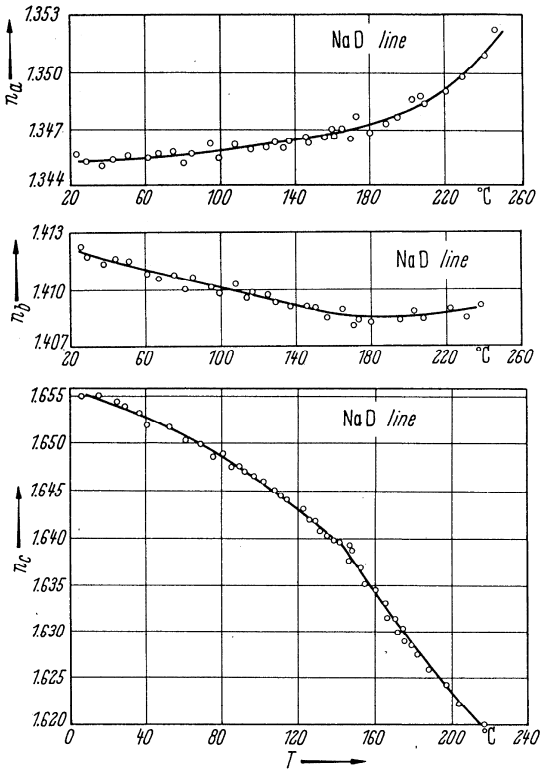

Fig. 28A-1-038. $NaNO_2$. n_a, n_b, n_c vs. T [66Hir].

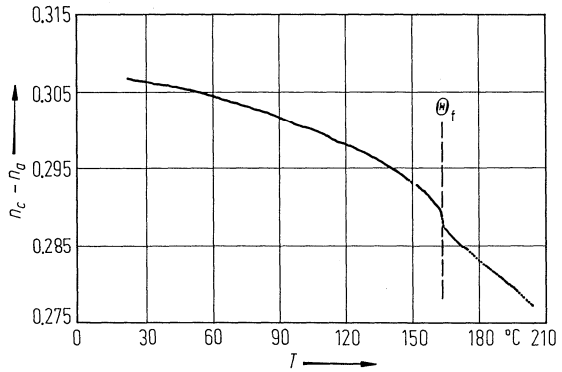

Fig. 28A-1-039. $NaNO_2$. $n_c - n_a$ vs. T [85Mit]. $\lambda = 632$ nm.

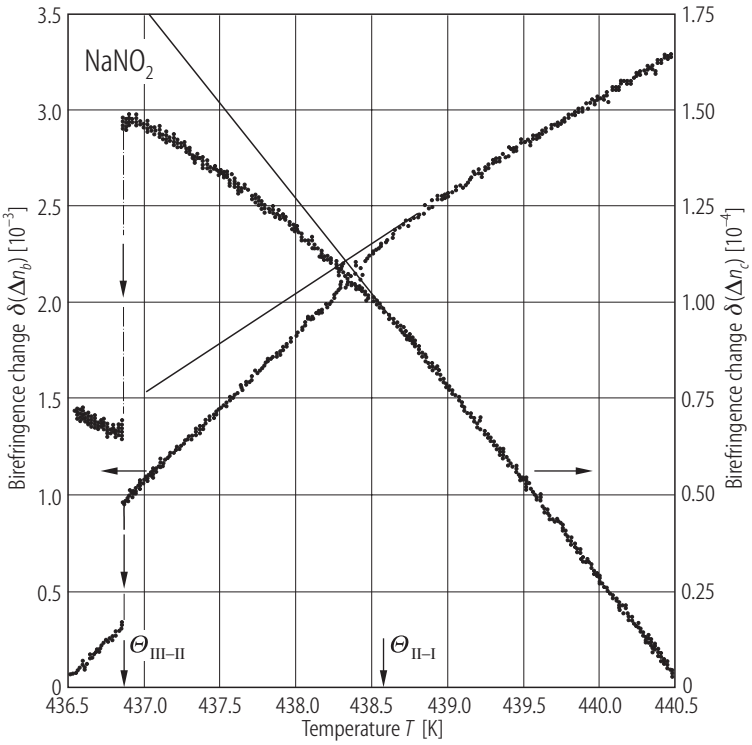

Fig. 28A-1-040. $NaNO_2$. $\delta(\Delta n_b)$, $\delta(\Delta n_c)$ vs. T in the vicinity of the III–II–I transitions [91Bia]. $\delta(\Delta n_b)$: $\Delta n_b(T) - \Delta n_b(436.5\ \text{K})$, $\delta(\Delta n_c)$: $\Delta n_c(T) - \Delta n_c(440.5\ \text{K})$.

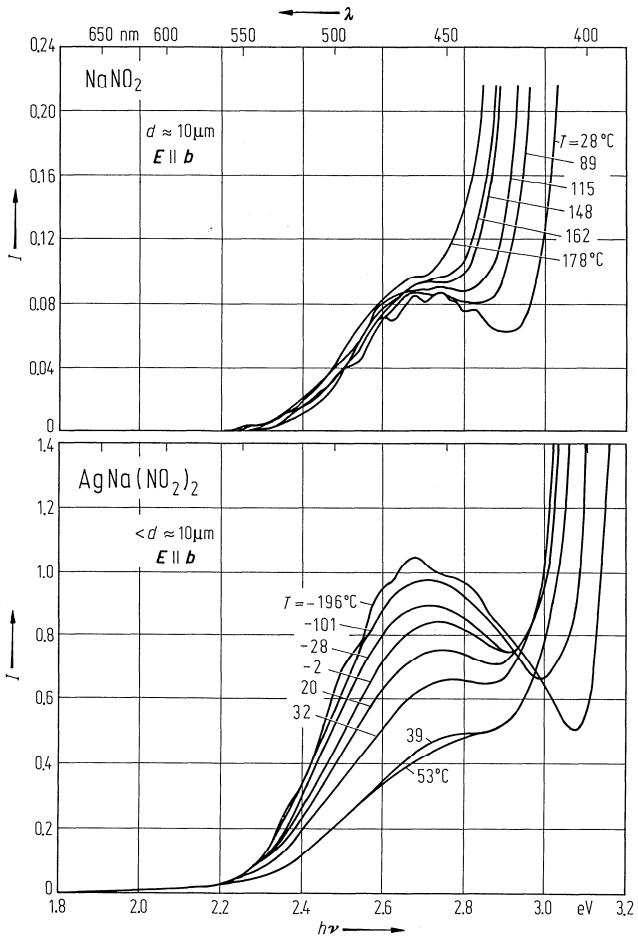

Fig. 28A-1-041. $NaNO_2$, $AgNa(NO_2)_2$. I vs. $h\nu$ [79Han]. Parameter: T. I: optical density. Sample thickness: ≈10 μm.

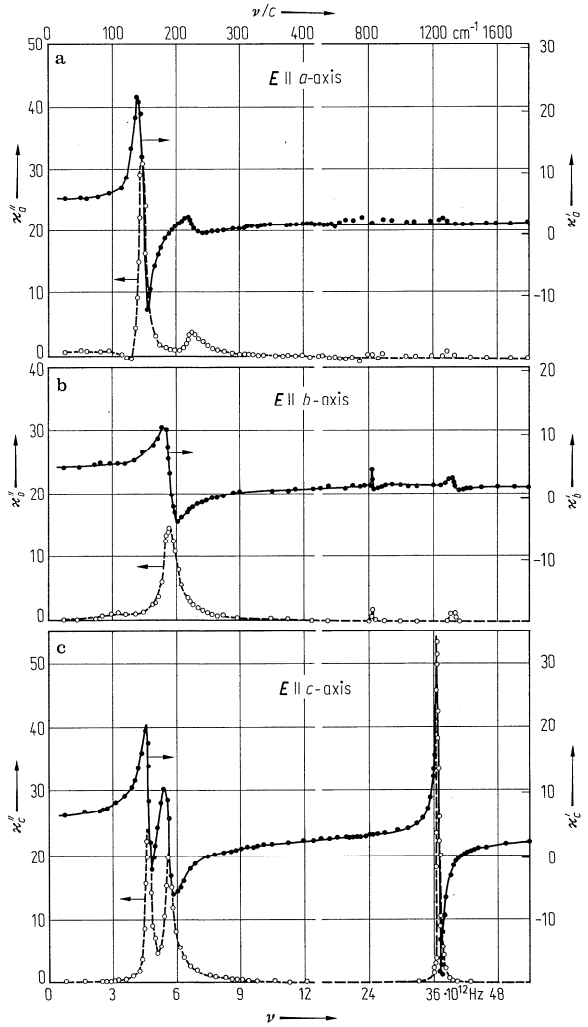

Fig. 28A-1-042. $NaNO_2$. κ', κ'' vs. ν [68Axe]. T = RT. Polarization of light: (**a**) || ***a***, (**b**) || ***b***, (**c**) || ***c***. Solid lines indicate κ' with the right scale, broken lines indicate κ'' with the left scale. Note change of scale at $\nu = 12 \cdot 10^{12}$ Hz.

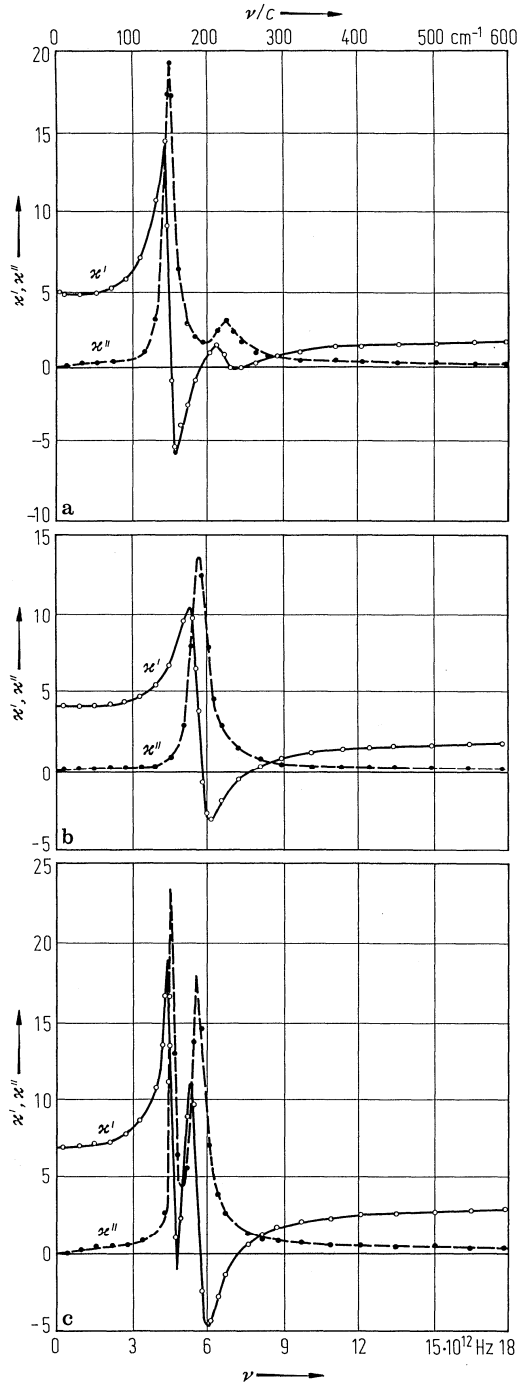

Fig. 28A-1-043. $NaNO_2$. κ', κ'' vs. ν [85Bre]. T = 293 K. (**a**) B_2 spectra with $\boldsymbol{E} \parallel \boldsymbol{a}$, (**b**) A_1 spectra with $\boldsymbol{E} \parallel \boldsymbol{b}$, (**c**) B_1 spectra with $\boldsymbol{E} \parallel \boldsymbol{c}$. κ' (solid curve) and κ'' (dashed curve) were obtained from the infrared reflectivity spectra.

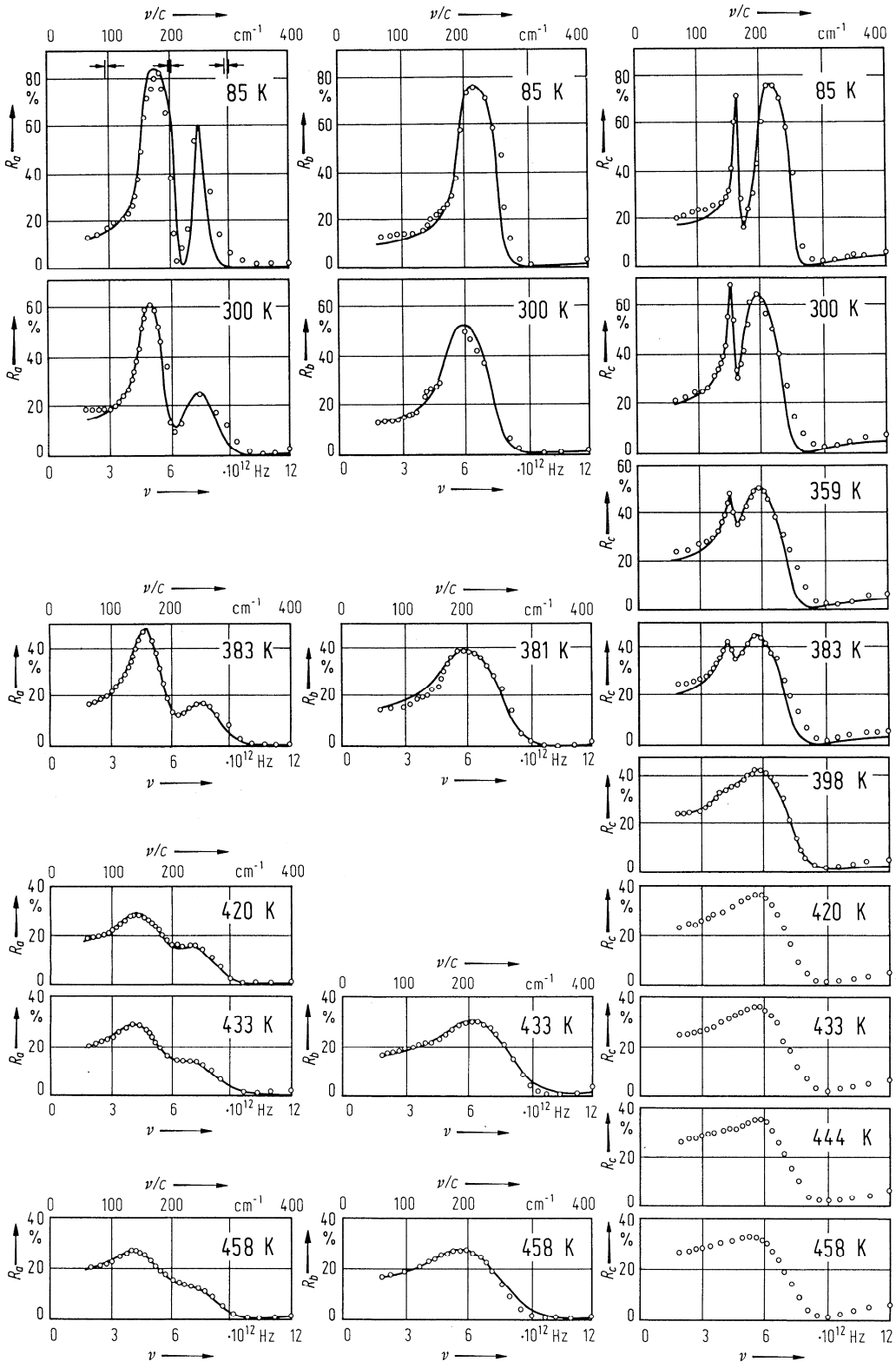

Fig. 28A-1-044. $NaNO_2$. R vs. ν [69Suz]. Along the a, b, c direction. R: reflectivity. Spectral resolution is indicated by gaps. Solid curves are calculated by using classical oscillation model.

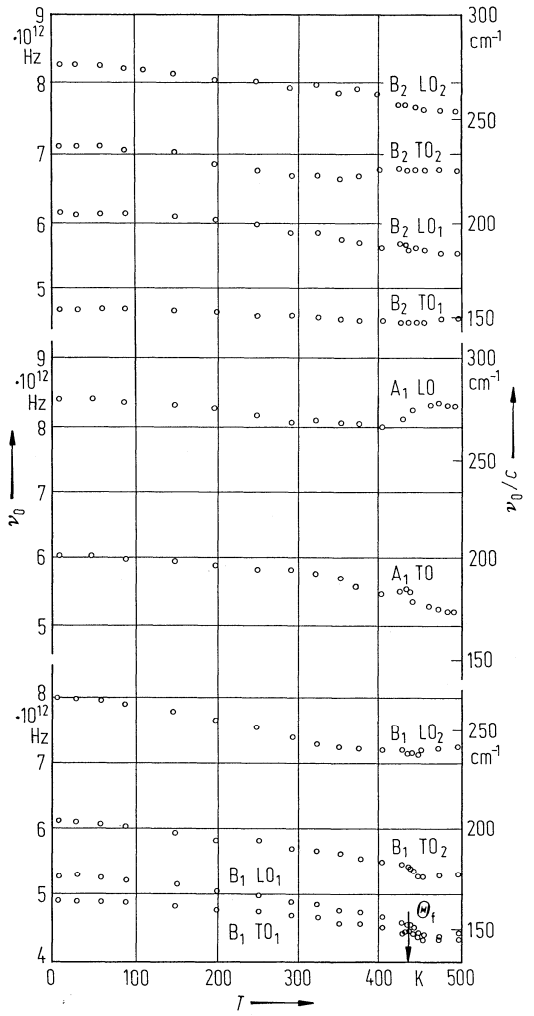

Fig. 28A-1-045. $NaNO_2$. ν_0 vs. T [85Bre]. ν_0: frequency of lattice modes.

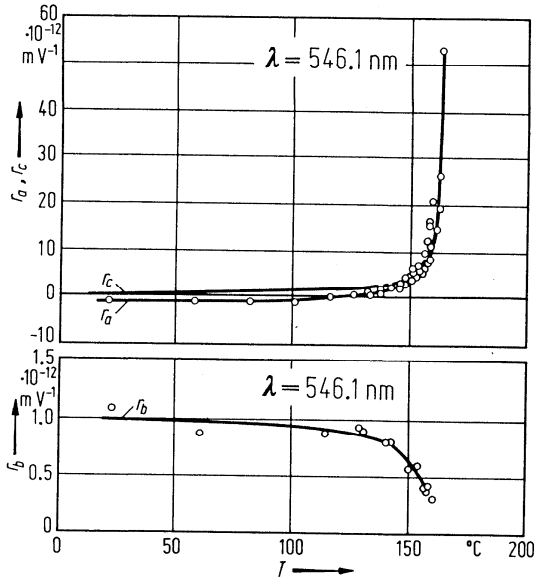

Fig. 28A-1-046. $NaNO_2$. r_a, r_b, r_c vs. T [69Joh]. $r_a = r_{22} - (n_3/n_2)^3 \cdot r_{32}$, $r_b = r_{32} - (n_1/n_3)^3 \cdot r_{12}$, $r_c = r_{22} - (n_1/n_2)^3 \cdot r_{12}$.

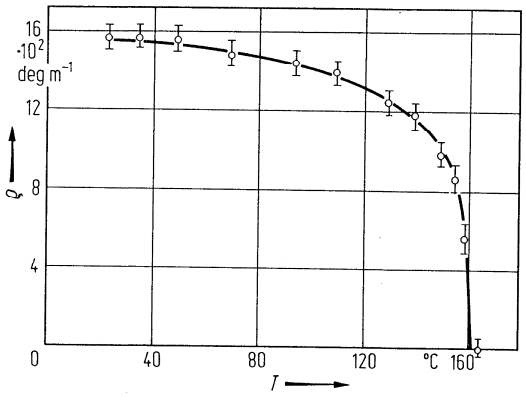

Fig. 28A-1-047. $NaNO_2$. ρ vs. T [72Che]. ρ: optical rotatory power.

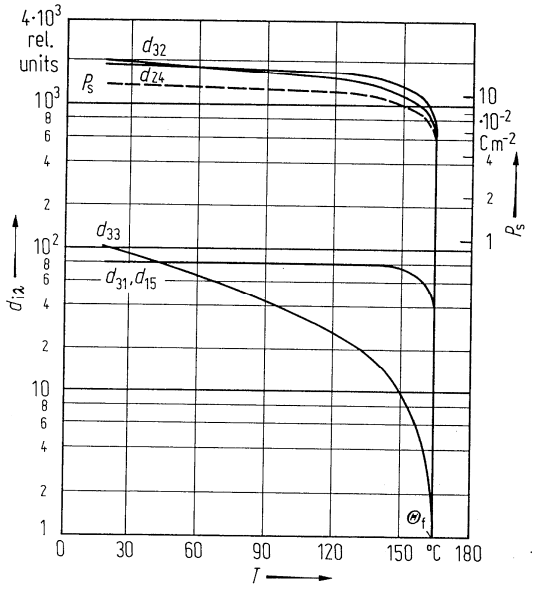

Fig. 28A-1-048. $NaNO_2$. $d_{i\lambda}$ vs. T [74Ino]. $d_{i\lambda}$: relative value of nonlinear optical susceptibility. P_s is also shown for comparison.

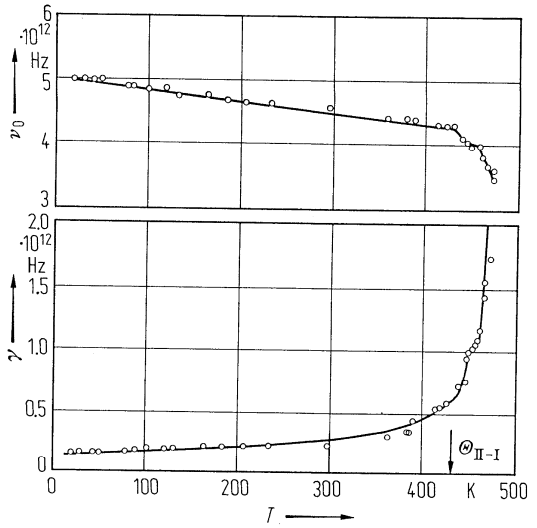

Fig. 28A-1-049. $NaNO_2$. ν_0, γ vs. T [73And]. ν_0: frequency of a B_1 phonon mode, γ: damping constant.

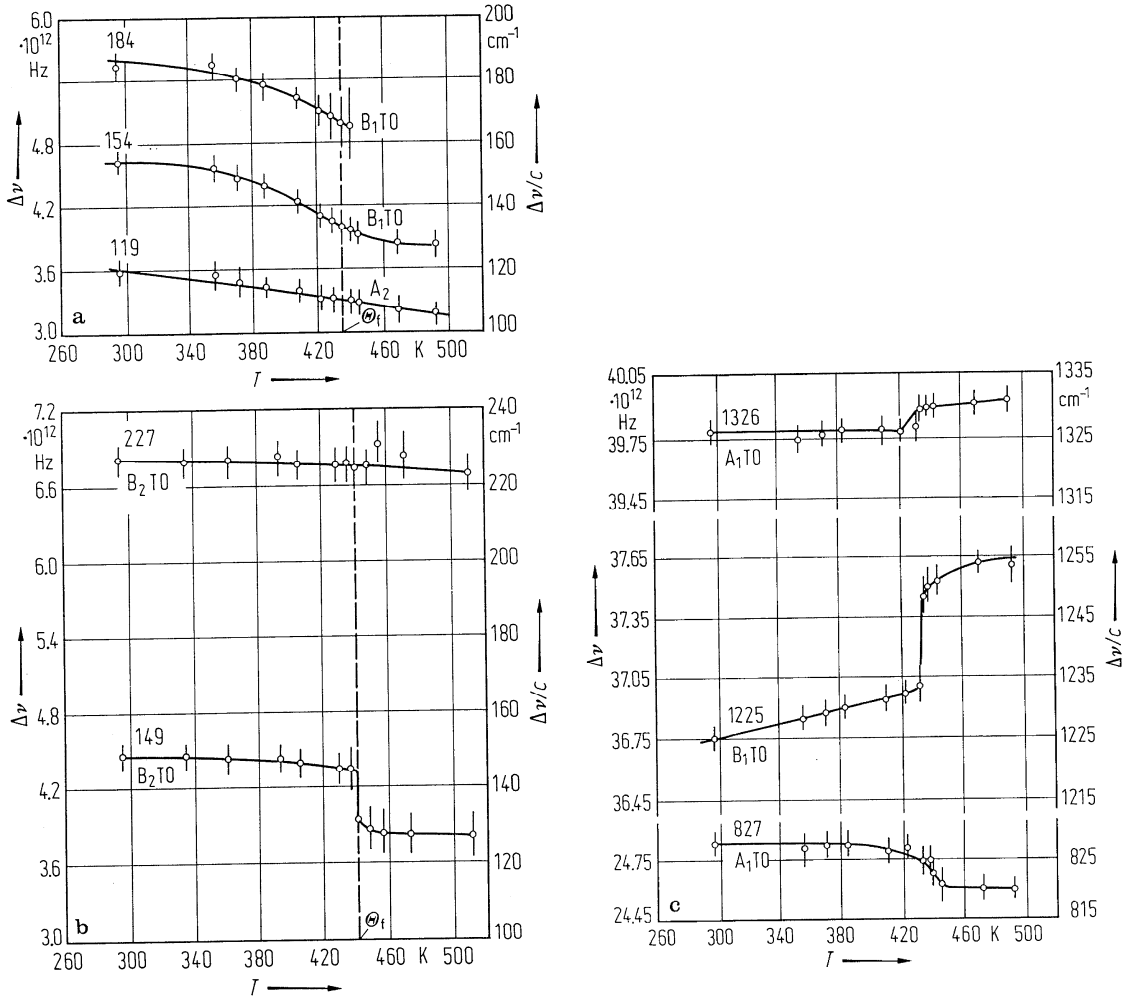

Fig. 28A-1-050. $NaNO_2$. $\Delta\nu$ vs. T [76Pra]. $\Delta\nu$: Raman frequency shift. (**a**), (**b**) for external modes, (**c**) for internal modes. Values of frequency shift at T = RT are given in figures in the unit of cm^{-1}. Vertical dashed lines indicate Θ_f.

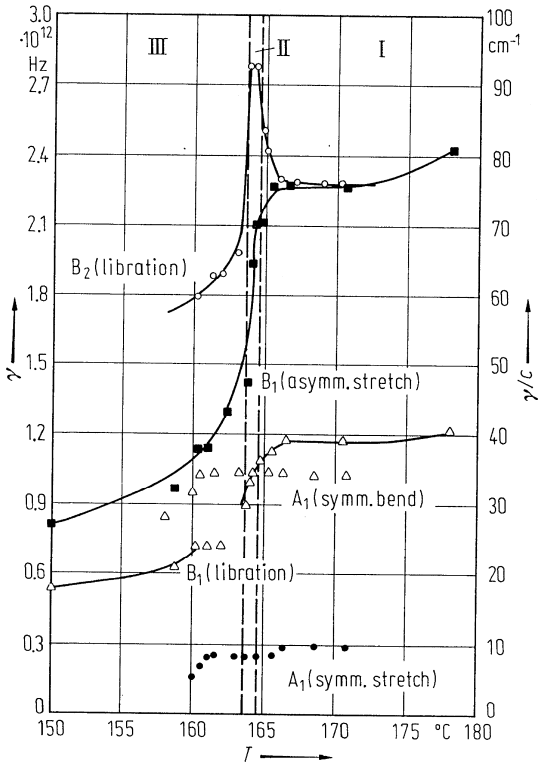

Fig. 28A-1-051. $NaNO_2$. γ vs. T [76Cas]. γ: full width at half maximum of Raman line. The dashed lines indicate the temperature range of phase II.

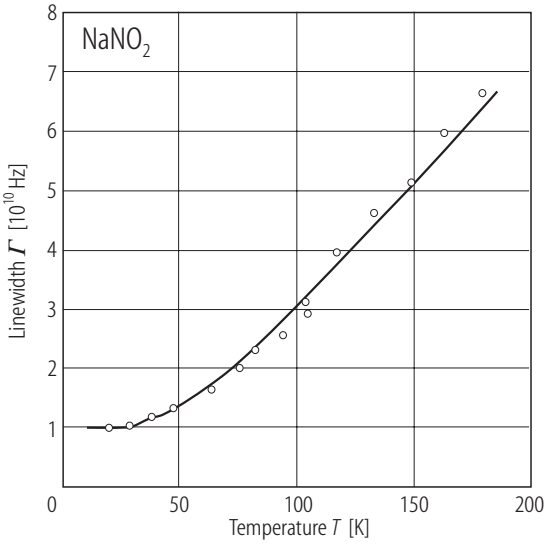

Fig. 28A-1-052. $NaNO_2$. Γ vs. T [89Bec]. Γ: linewidth of B_1 TO phonon mode Raman line.

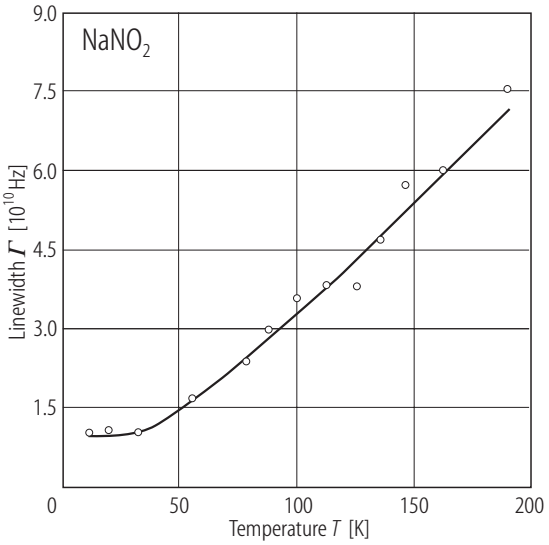

Fig. 28A-1-053. $NaNO_2$. Γ vs. T [89Bec]. Γ: linewidth of A_2 lattice mode Raman line.

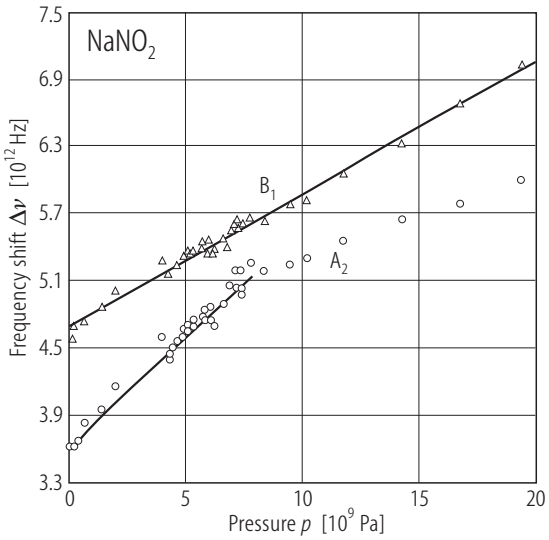

Fig. 28A-1-054. $NaNO_2$. $\Delta\nu$ vs. p [89Dal]. T = RT. $\Delta\nu$: Raman frequency shift of libration modes.

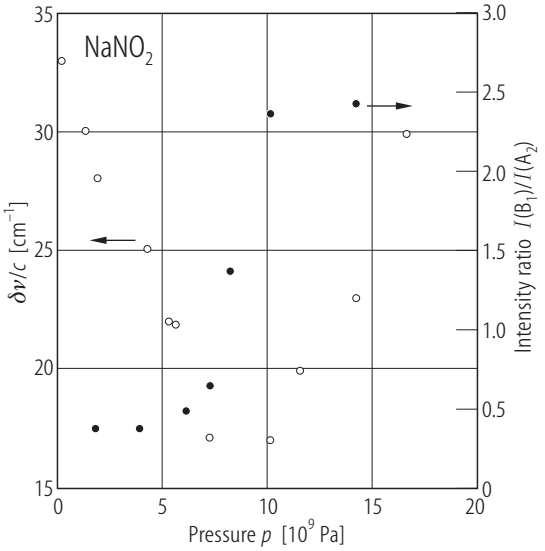

Fig. 28A-1-055. $NaNO_2$. $\delta\nu/c$, $I(B_1)/I(A_2)$ vs. p [89Dal]. T = RT. $\delta\nu$: difference of Raman frequency of B_1 and A_2 lattice modes. $I(B_1)/I(A_2)$: relative intensity of B_1 mode line to A_2 mode line.

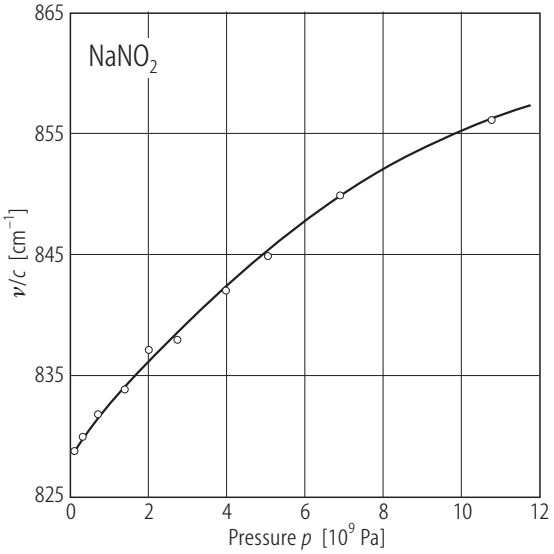

Fig. 28A-1-056. $NaNO_2$. ν/c vs. p [89Dal]. T = RT. ν: frequency of internal A bending mode of NO_2^-.

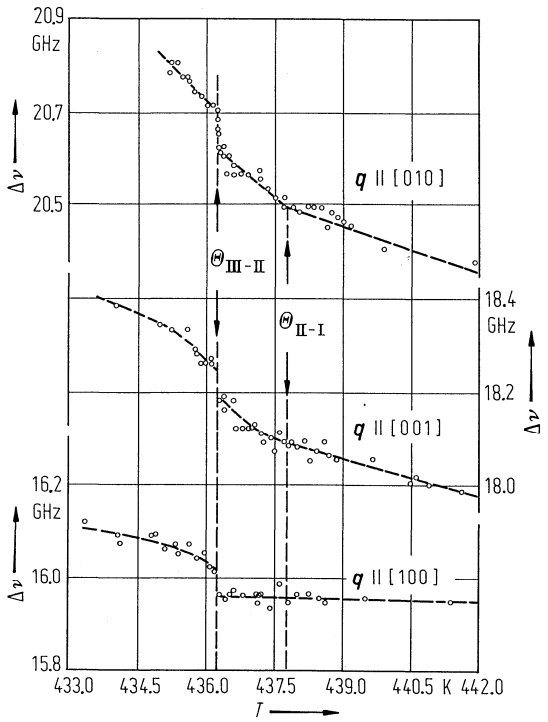

Fig. 28A-1-057. $NaNO_2$. $\Delta\nu$ vs. T for different q [82Yag]. $\Delta\nu$: Brillouin scattering frequency shift of longitudinal waves. q: scattering vector.

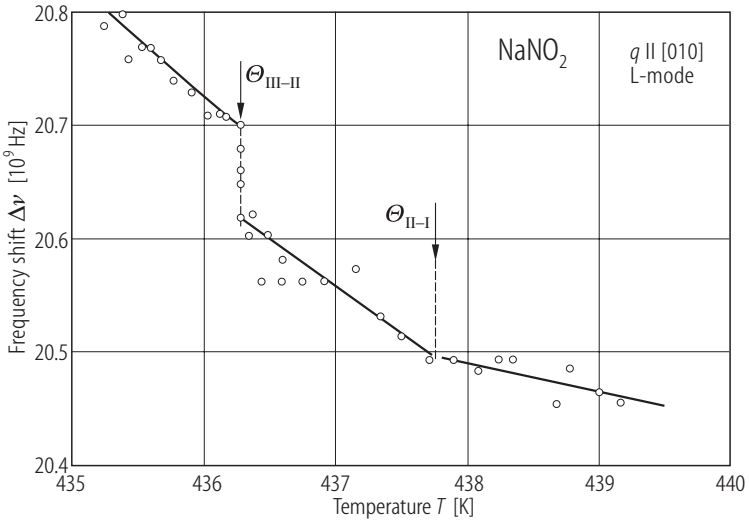

Fig. 28A-1-058. $NaNO_2$. $\Delta\nu$ vs. T in the vicinity of the III–II–I transitions [80Yag]. $\Delta\nu$: Brillouin frequency shift of longitudinal acoustic mode propagation along the b direction.

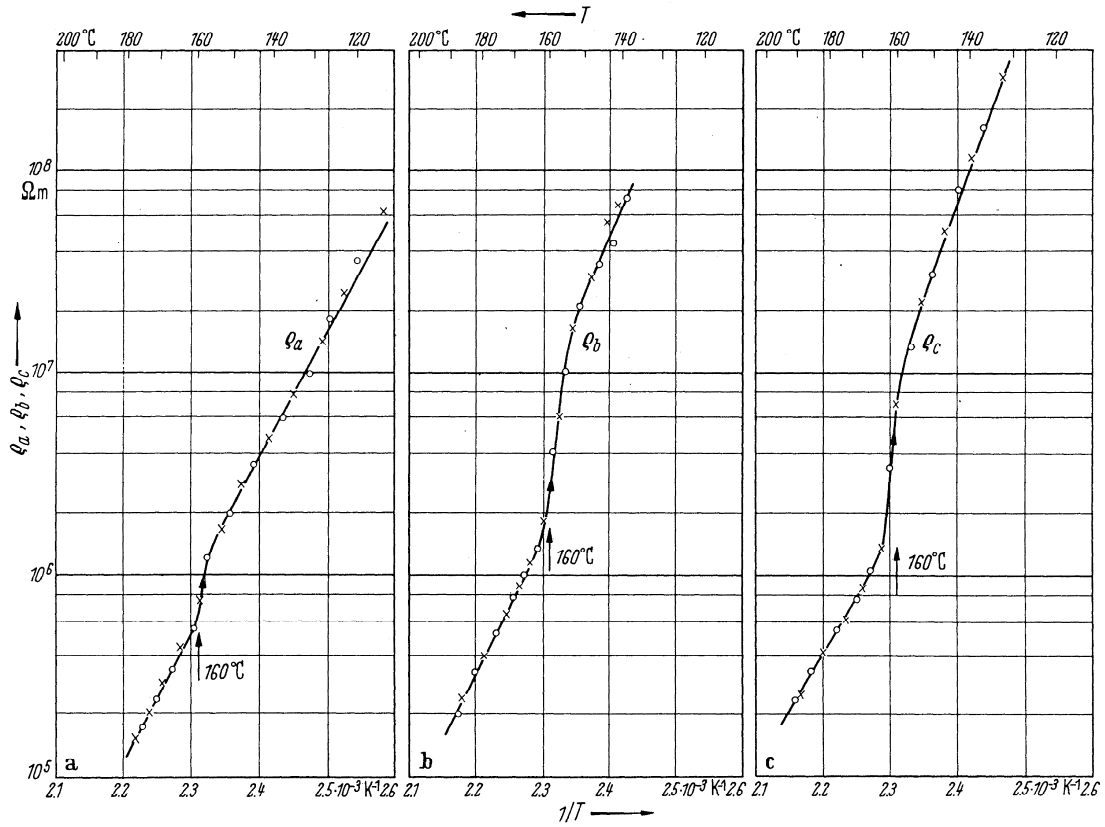

Fig. 28A-1-059. $NaNO_2$. (**a**) ρ_a, (**b**) ρ_b, (**c**) ρ_c vs. $1/T$ [62Asa].

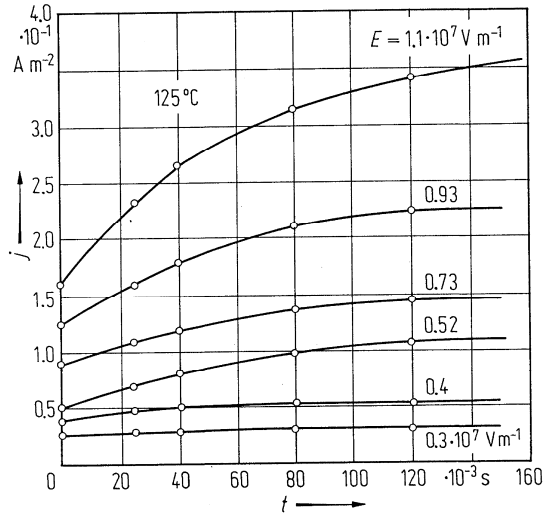

Fig. 28A-1-060. $NaNO_2$. j vs. t [72Fok]. Parameter: E. T = 125 °C. j: current density along the b direction, E: field strength of pulse.

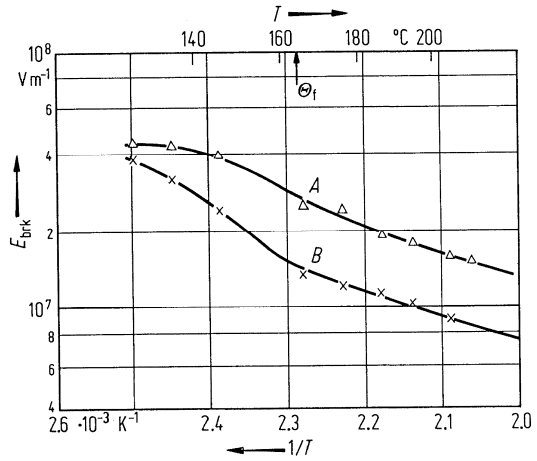

Fig. 28A-1-061. $NaNO_2$. E_{brk} vs. $1/T$ [72Fok]. E_{brk}: breakdown field. Curve *A*: for time to breakdown of 0.01 s, curve *B*: 0.1 s. A single flat-topped voltage pulse having a rise-time of 10^{-3} s is applied along the *b* direction.

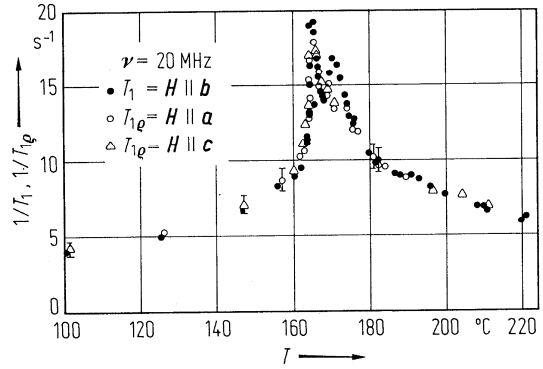

Fig. 28A-1-062. $NaNO_2$. $1/T_1$, $1/T_{1\rho}$ vs. T [75Avo]. T_1: spin-lattice relaxation time of ^{23}Na. $T_{1\rho}$: spin-lattice relaxation time for ^{23}Na in the rotating frame.

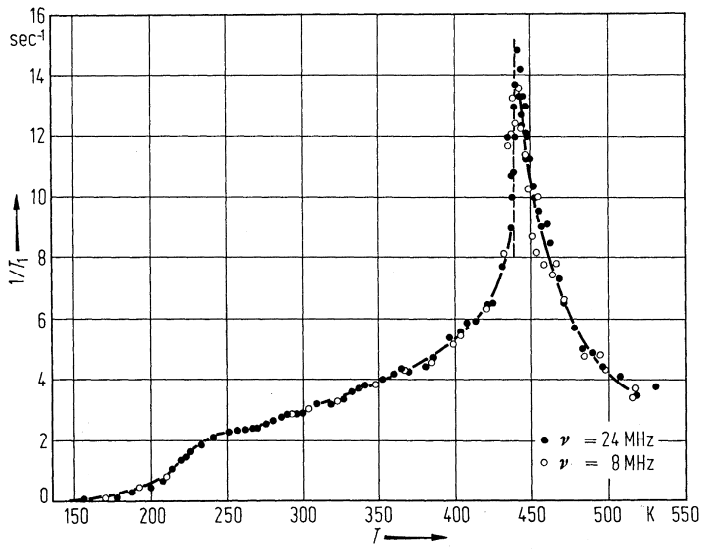

Fig. 28A-1-063. $NaNO_2$. $1/T_1$ vs. T [70Bon]. T_1: spin-lattice relaxation time of ^{23}Na.

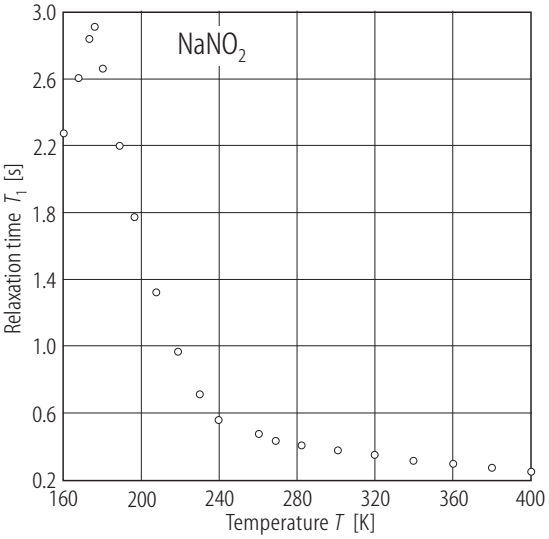

Fig. 28A-1-064. $NaNO_2$. T_1 vs. T [93Han]. T_1: spin-lattice relaxation time of ^{23}Na.

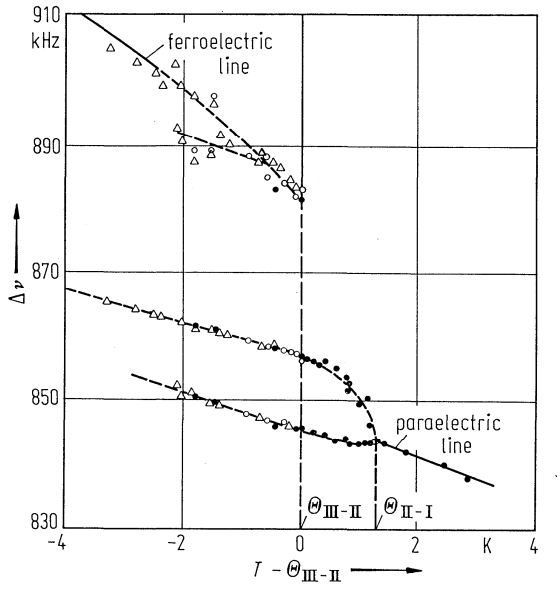

Fig. 28A-1-065. $NaNO_2$. $\Delta\nu$ vs. $T - \Theta_{III-II}$ [81Buc1]. $\Delta\nu$: ^{23}Na NMR satellite splitting. $\boldsymbol{H} \parallel \boldsymbol{b}$. ν_L = 23.81 MHz. Results from different samples and different temperature runs.

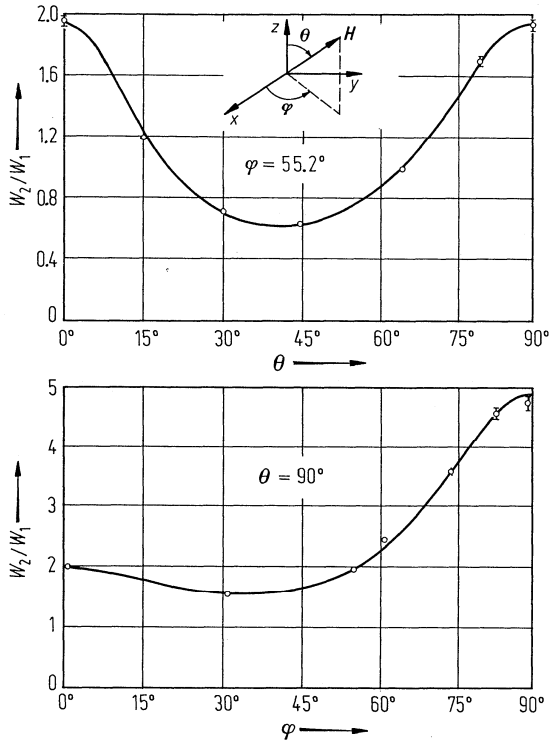

Fig. 28A-1-066. $NaNO_2$. W_2/W_1 vs. θ, φ [82Hug]. W_2/W_1: ratio of ^{23}Na nuclear transition probability for $\Delta m = \pm 1$ and ± 2. θ, φ: polar coordinates.

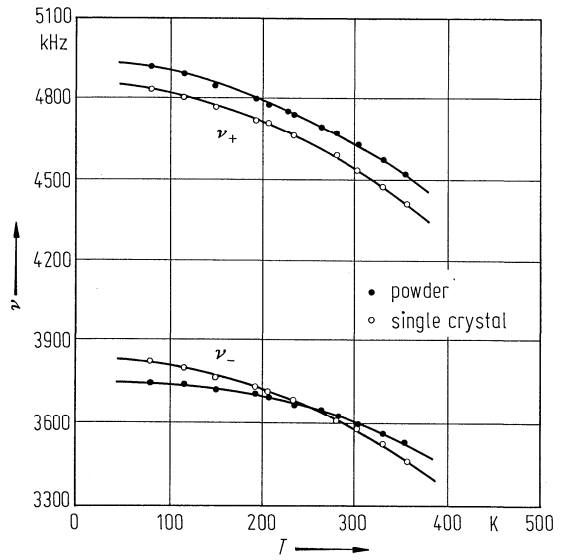

Fig. 28A-1-067. $NaNO_2$. ν vs. T [81Cho]. ν: frequency of ^{14}N NQR line.

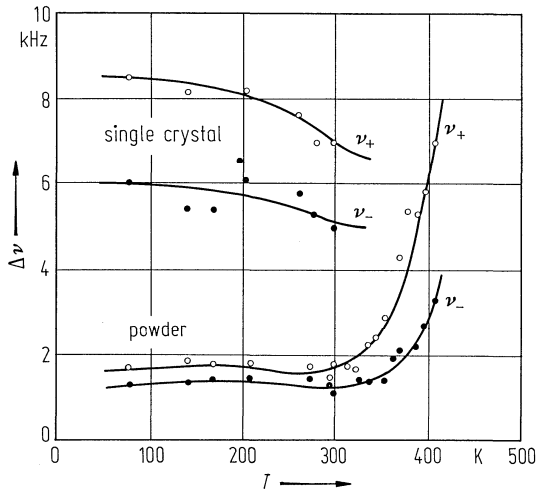

Fig. 28A-1-068. $NaNO_2$. $\Delta\nu$ vs. T [81Cho]. $\Delta\nu$: linewidth of ^{14}N NQR line.

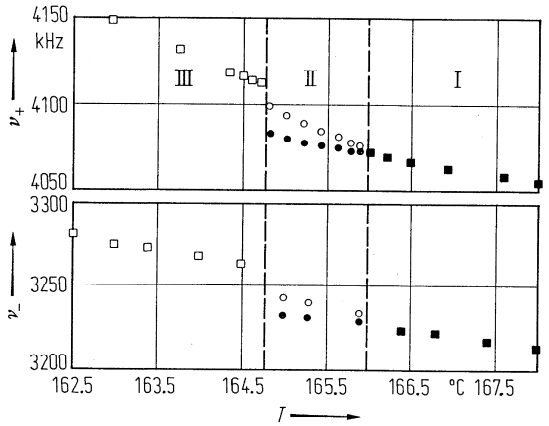

Fig. 28A-1-069. $NaNO_2$. $\nu_{\pm}$ vs. T [77Amb]. ν_+, ν_-: ^{14}N NQR frequencies.

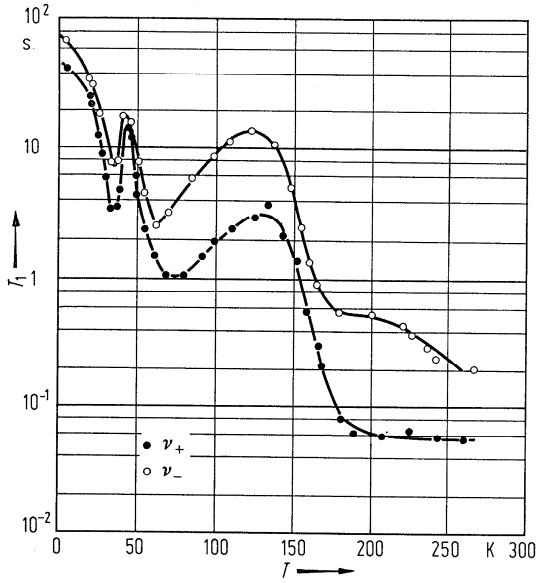

Fig. 28A-1-070. $NaNO_2$. T_1 vs. T [72Abe]. T_1: spin-lattice relaxation time of ^{14}N. $\nu_+ = (1/4)(eQ\phi_{zz}/h)\cdot(3 + \eta)$, $\nu_- = (1/4)(eQ\phi_{zz}/h)\cdot(3 - \eta)$.

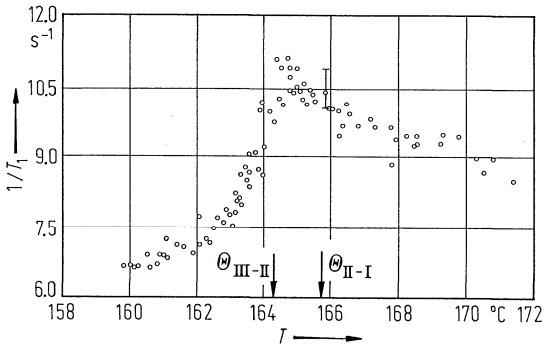

Fig. 28A-1-071. $NaNO_2$. $1/T_1$ vs. T in the vicinity of the III–II–I transitions [81Buc2]. T_1: ^{23}Na spin-lattice relaxation time. $\boldsymbol{H} \parallel \boldsymbol{b}$.

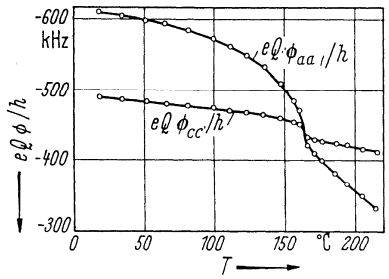

Fig. 28A-1-072. $NaNO_2$. $eQ\phi_{aa}/h$, $eQ\phi_{cc}/h$ vs. T [62Wei]. ϕ_{ii}: field gradient tenor component for ^{23}Na.

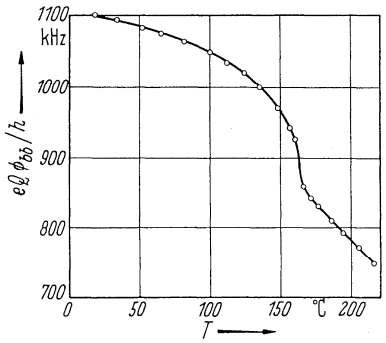

Fig. 28A-1-073. $NaNO_2$. $eQ\phi_{bb}/h$ vs. T [62Wei]. ϕ_{bb}: field gradient tensor component for ^{23}Na.

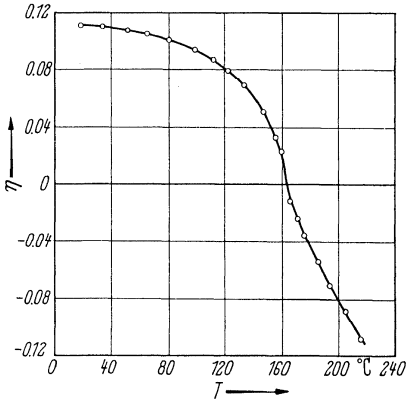

Fig. 28A-1-074. $NaNO_2$. η vs. T [62Wei]. η: asymmetry parameter for ^{23}Na, $\eta = (\phi_{cc} - \phi_{aa})/\phi_{bb}$.

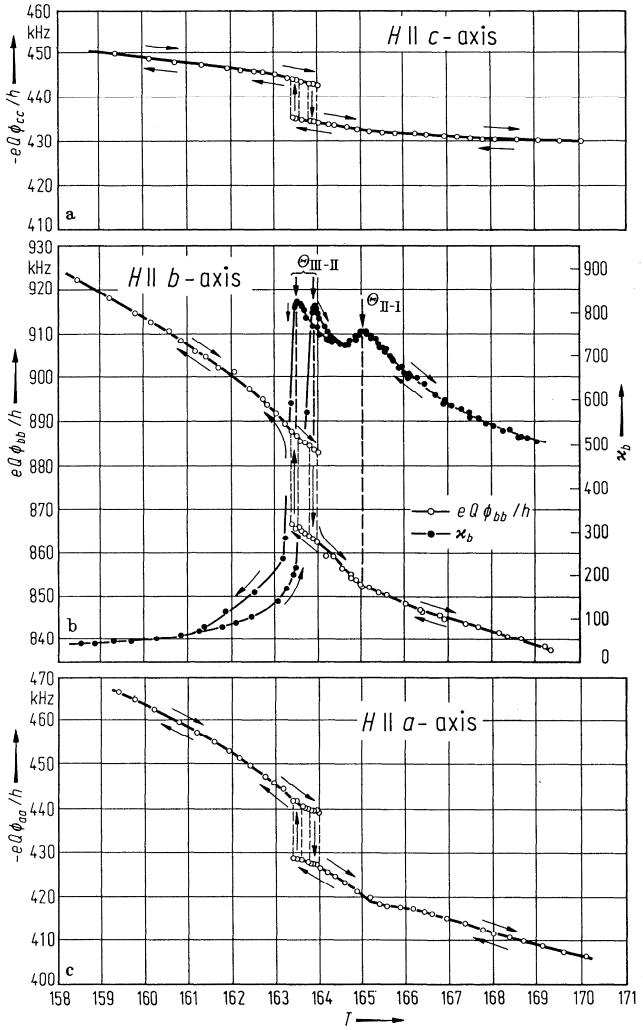

Fig. 28A-1-075. $NaNO_2$. $eQ\phi_{ii}/h$ vs. T in the vicinity of the III–II–I transitions [70Yag]. (**a**) $-eQ\phi_{cc}/h$, (**b**) $eQ\phi_{bb}/h$, (**c**) $-eQ\phi_{aa}/h$ for ^{23}Na. In (**b**), κ_b at f = 1.5 kHz vs. T is also shown. ϕ_{ii}: field gradient tensor component.

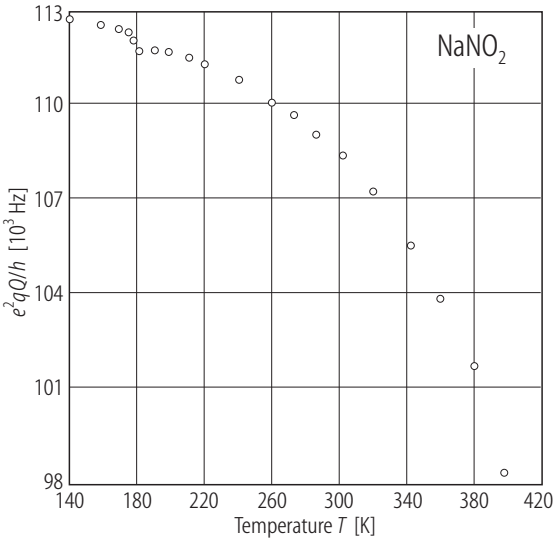

Fig. 28A-1-076. $NaNO_2$. e^2qQ/h vs. T [93Han]. e^2qQ/h: quadrupole coupling constant for ^{23}Na.

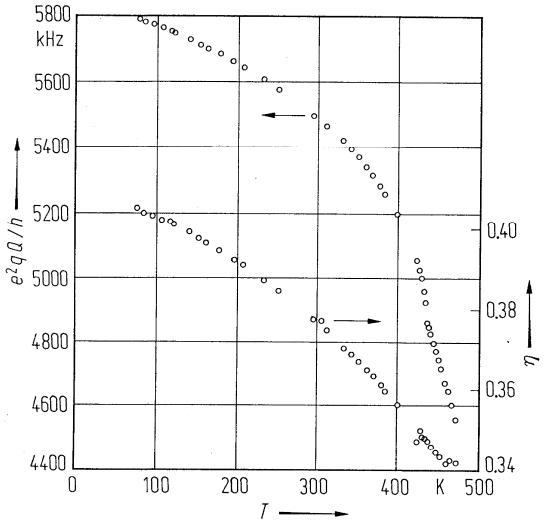

Fig. 28A-1-077. $NaNO_2$. e^2qQ/h, η vs. T [76Pet]. η: asymmetry parameter of field gradient tensor for ^{14}N.

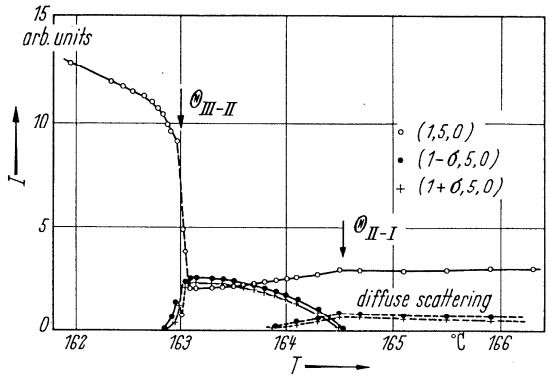

Fig. 28A-1-078. $NaNO_2$. $I_{(1,5,0)}$, $I_{satellite}$ vs. T [67Hos]. $I_{(1,5,0)}$: intensity of (1,5,0) X-ray reflection, $I_{satellite}$: intensity of satellite reflection due to structural modulation.

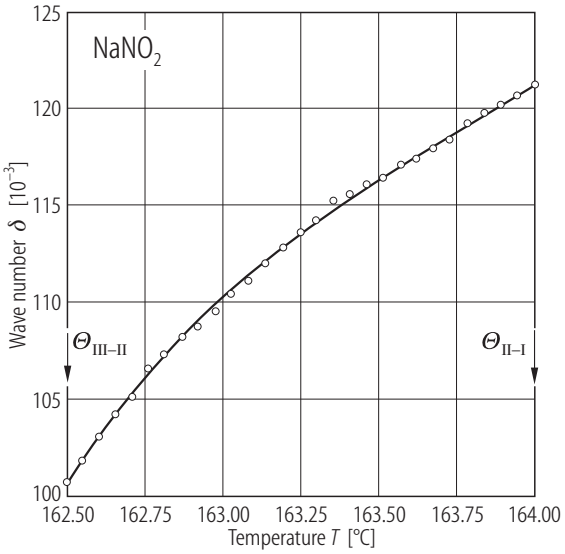

Fig. 28A-1-079. $NaNO_2$. δ vs. T in phase II [82Dur]. δ: wave number of structural modulation along the a direction in phase II in units of a^*.

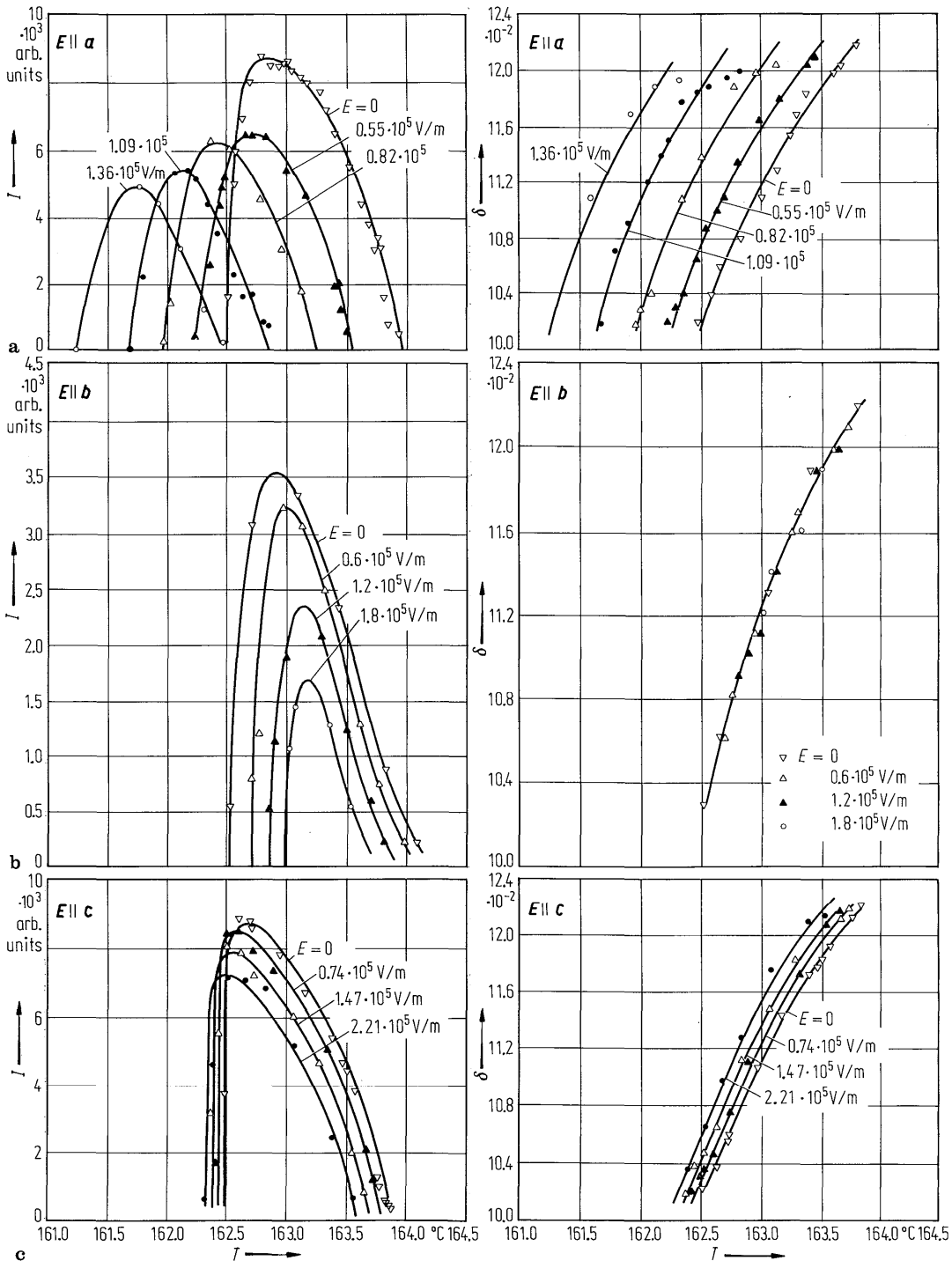

Fig. 28A-1-080. $NaNO_2$. δ, I vs. T in phase II. Parameter: E. (**a**) $\boldsymbol{E} \parallel \boldsymbol{a}$ [86Qiu], (**b**) $\boldsymbol{E} \parallel \boldsymbol{b}$ [83Qiu], (**c**) $\boldsymbol{E} \parallel \boldsymbol{c}$ [86Qiu]. δ: wave number of lattice modulation along the a direction in units of a^*. I: intensity of neutron satellite reflection due to the lattice modulation.

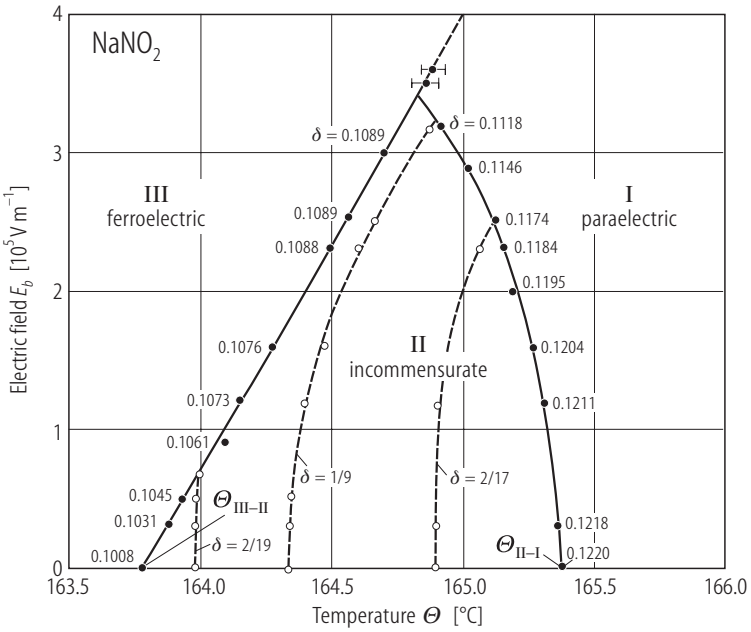

Fig. 28A-1-081. $NaNO_2$. $\Theta - E_b$ phase diagram together with equal δ-lines [83Dur]. δ: wave number of lattice modulation along the a direction in units of a^*. The equal δ-lines are shown as dashed curves. δ-values at phase boundaries are also shown.

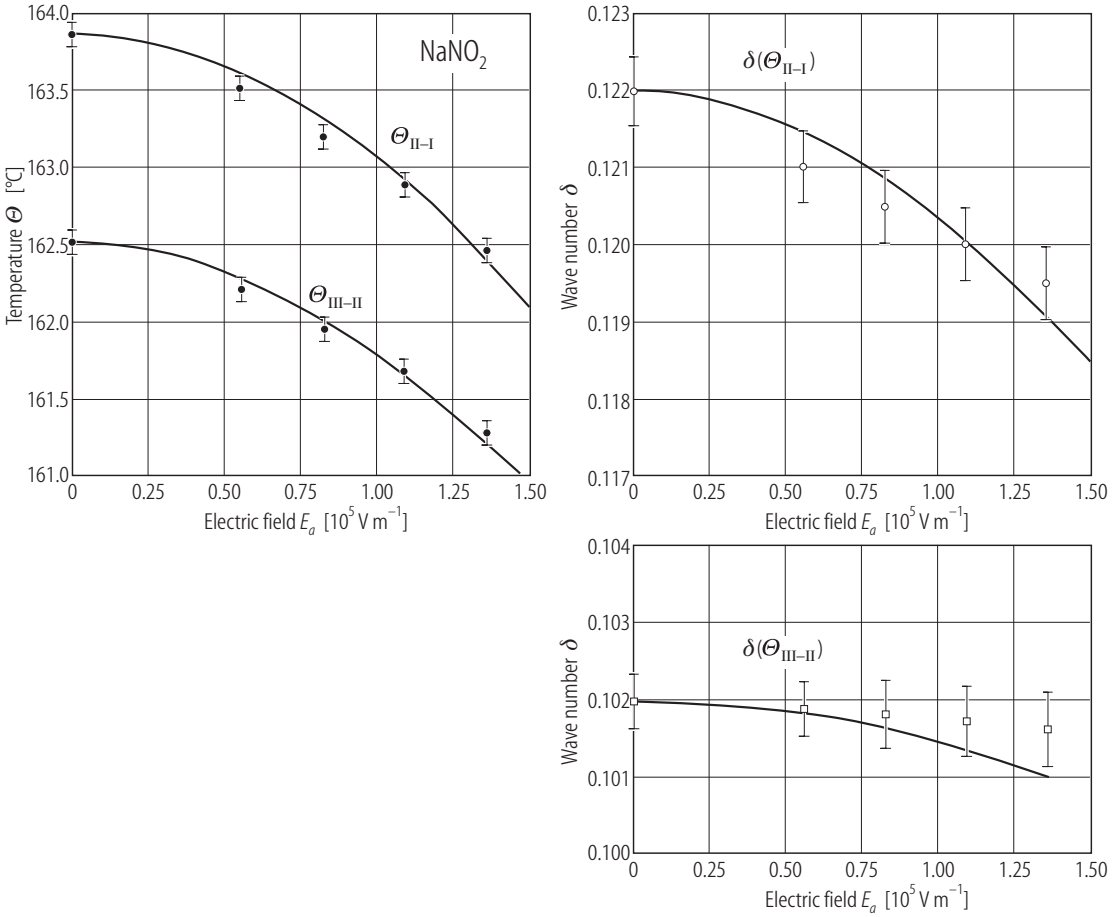

Fig. 28A-1-082. $NaNO_2$. Θ, $\delta(\Theta_{III-II})$, $\delta(\Theta_{II-I})$ vs. E_a in the vicinity of phase II [87Cum]. $\delta(\Theta_{III-II})$, $\delta(\Theta_{II-I})$: wave number of lattice modulation along the a direction in units of a^* at Θ_{III-II} and Θ_{II-I}, respectively.

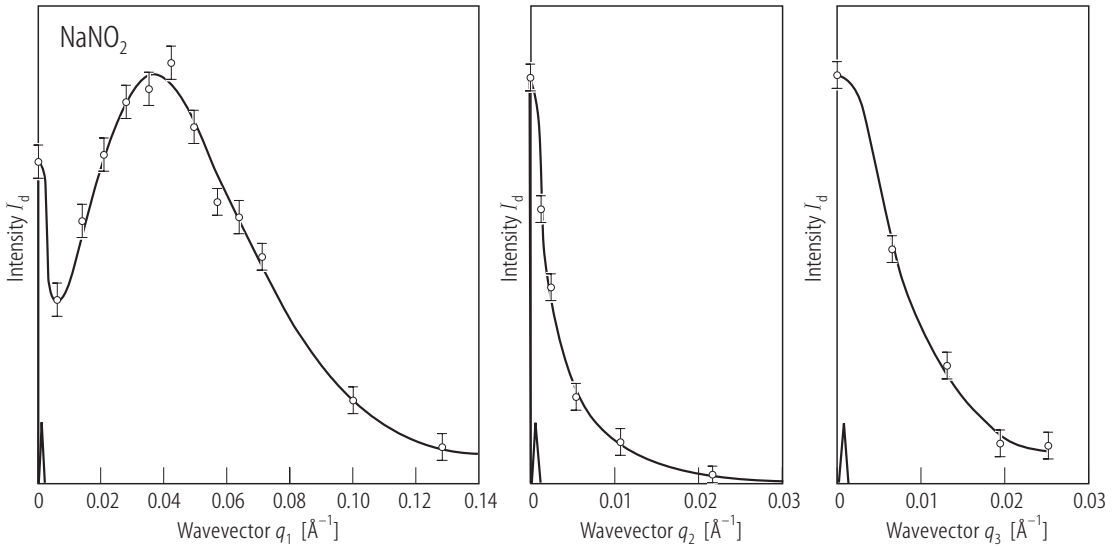

Fig. 28A-1-083. $NaNO_2$. I_d vs. q_i (i = 1, 2, 3) [66Yam]. $T = \Theta_{II-I} + 3$ K. I_d: diffuse scattering intensity. q_i: component of wave number vector. Triangles indicate the resolution functions. The peak at $q_1 = 0$ includes the contribution of the normal Bragg reflection.

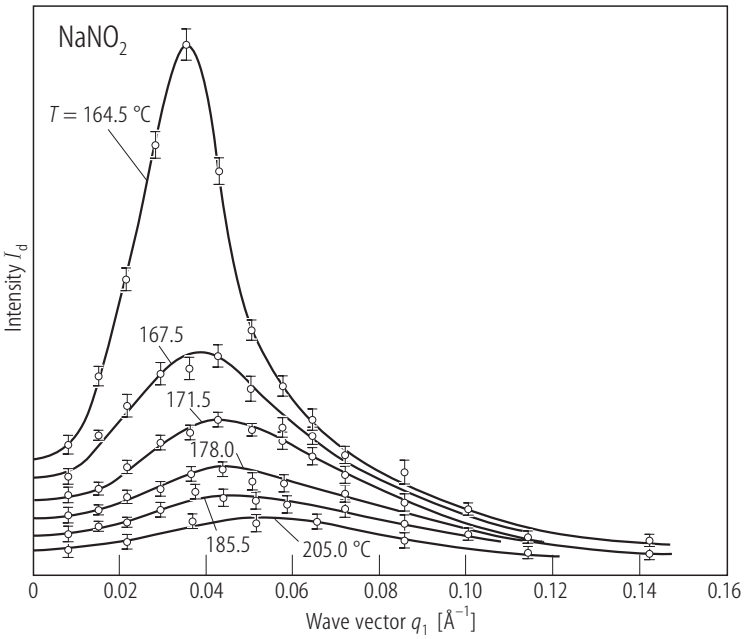

Fig. 28A-1-084. $NaNO_2$. I_d vs. q_1 [66Yam]. Parameter: T. I_d: diffuse scattering intensity. q_1: a^* component of wave number vector.

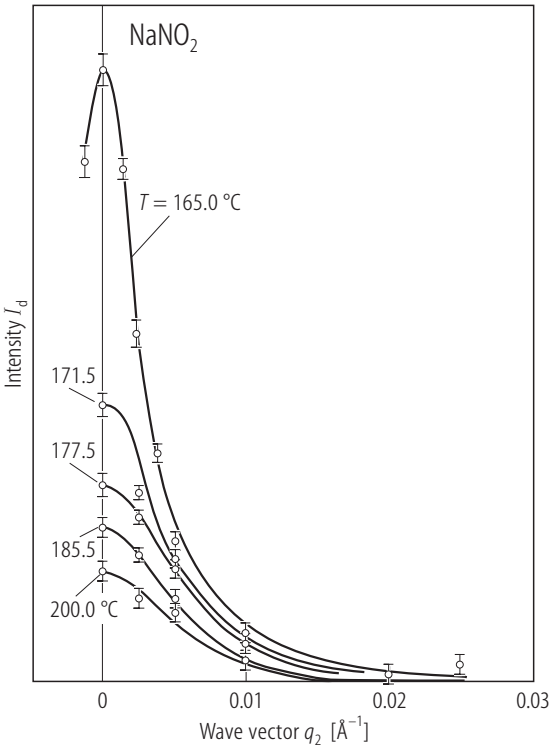

Fig. 28A-1-085. $NaNO_2$. I_d vs. q_2 [66Yam]. Parameter: T. I_d: diffuse scattering intensity. q_2: b^* component of wave number vector.

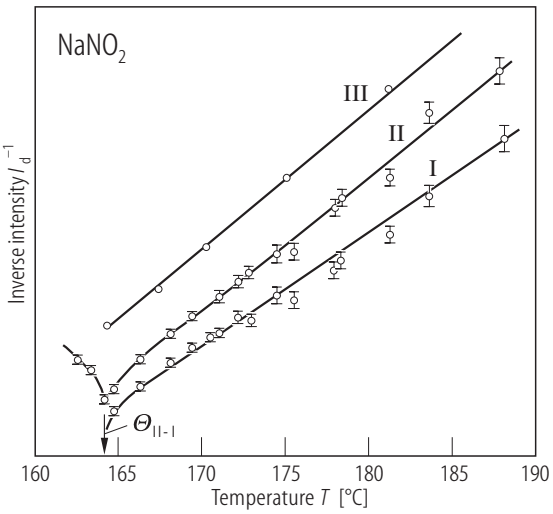

Fig. 28A-1-086. $NaNO_2$. $1/I_d(q)$ vs. T [66Yam]. $I_d(q)$: diffuse scattering intensity at wave number q. I: $q = q_s$, II: $q = q_s + 0.1a^*$, III: $q = 0$. q_s: wave number vector which gives the maximum diffuse scattering intensity.

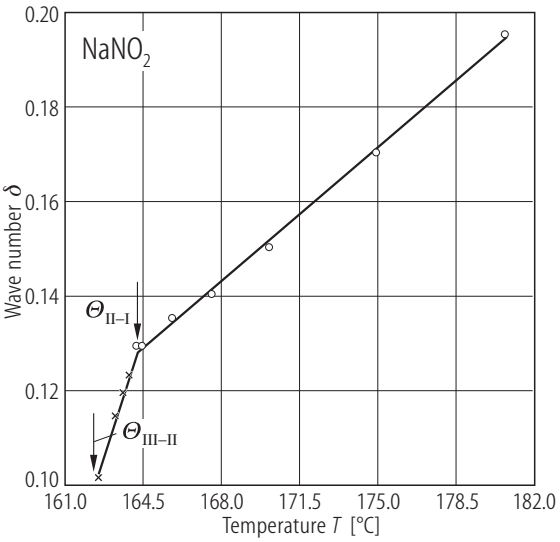

Fig. 28A-1-087. $NaNO_2$. δ vs. T in phase I [86Qiu]. δ: wave number of diffuse scattering peak along the a direction in units of a^*. Cross: δ of satellite reflection in phase II.

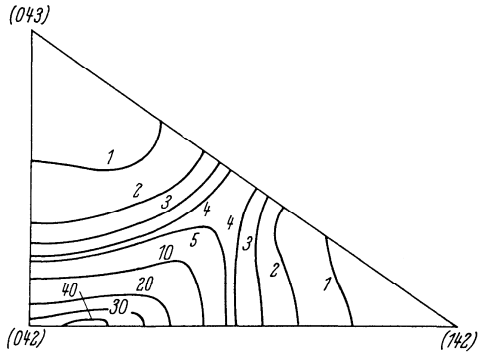

Fig. 28A-1-088. $NaNO_2$. Distribution of diffuse scattering intensity vertical to b^* divided by B^2 near (042) [63Tan]. B^2: structure factor (see original paper).

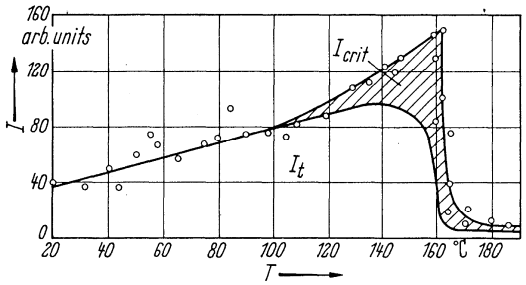

Fig. 28A-1-089. $NaNO_2$. I_{crit} , I_t vs. T at (1 ± 0.02, 3 ± 0.05, 0) [61Shi]. I_{crit}: X-ray critical scattering intensity, I_t: thermal diffuse scattering intensity.

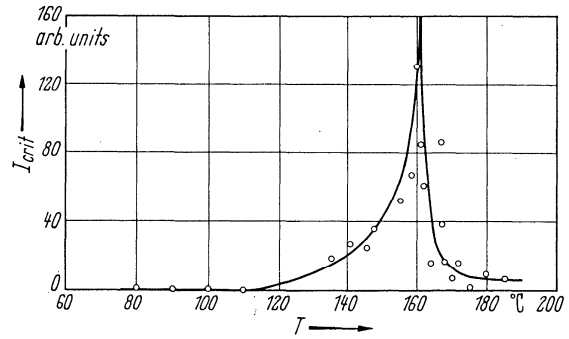

Fig. 28A-1-090. $NaNO_2$. I_{crit} vs. T [61Shi]. I_{crit}: critical scattering intensity at (1 ± 0.02, 3 ± 0.05, 0).

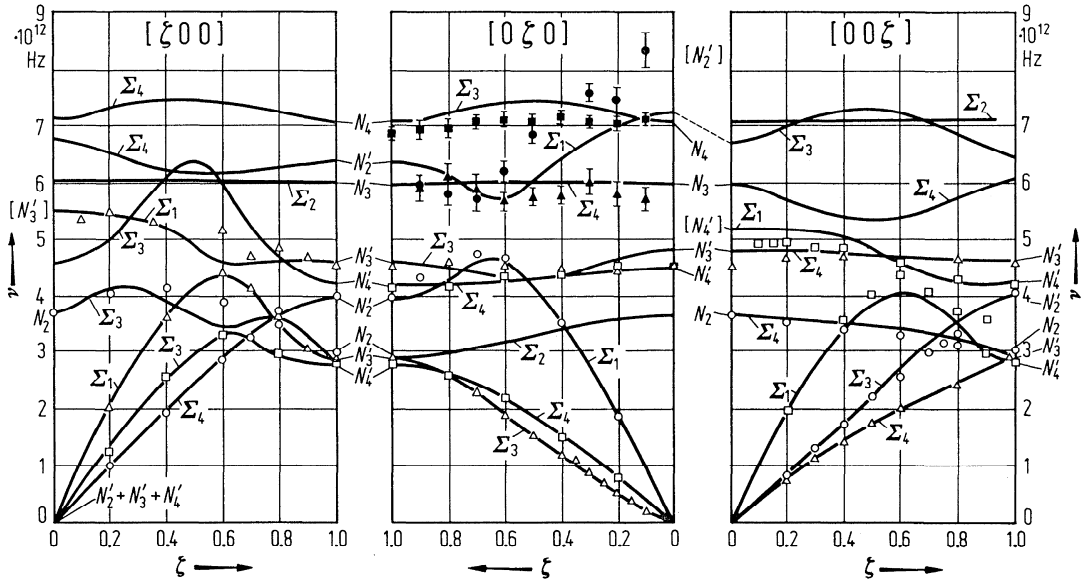

Fig. 28A-1-091. $NaNO_2$. ν vs. ζ [70Sak]. ν: phonon frequency, ζ: reduced wave vector coordinate. Open figures: at 23 °C, solid figures: at –163 °C.

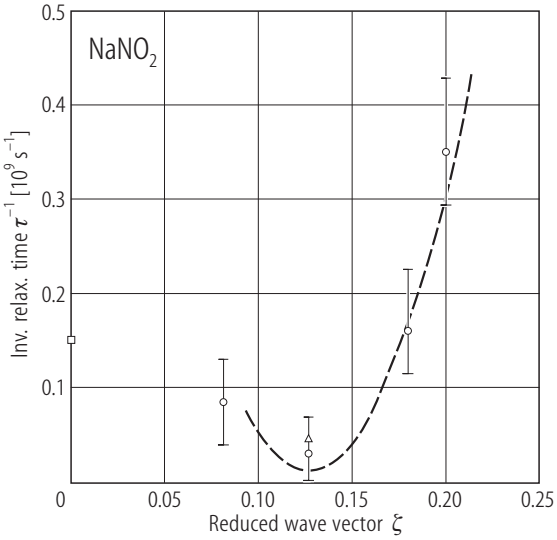

Fig. 28A-1-092. $NaNO_2$. $1/\tau$ vs. ζ [89Dur]. $T = \Theta_{II-I} + 0.3$ K. τ: relaxation time of pretransitional fluctuation. ζ: reduced wave vector coordinate along a^*. Triangle: result of ultrasonic measurement [86HuJ], square: result of dielectric measurement [70Hat].

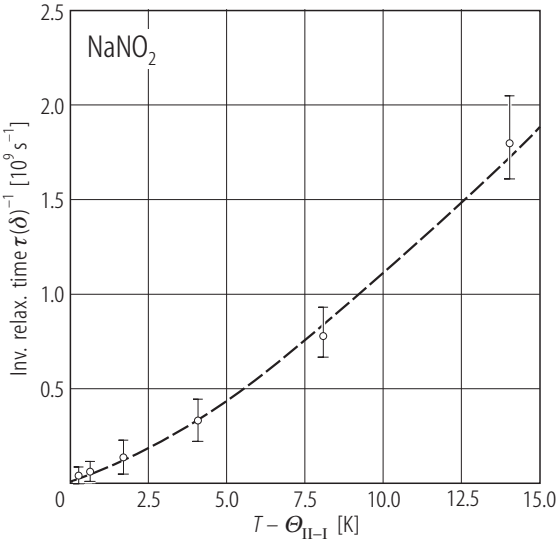

Fig. 28A-1-093. $NaNO_2$. $1/\tau(\delta)$ vs. $T - \Theta_{II-I}$ [89Dur]. $\tau(\delta)$: critical relaxation time at the wave vector of lattice modulation.

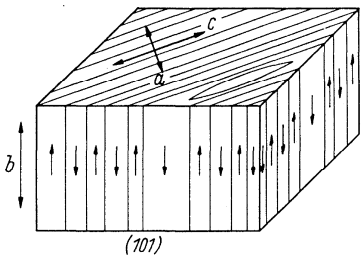

Fig. 28A-1-094. $NaNO_2$. Schematic representation of domain structure [61Nom2].

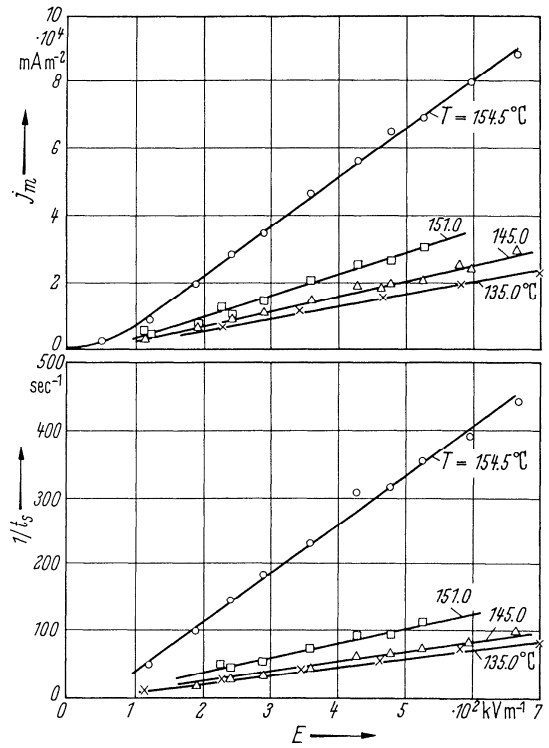

Fig. 28A-1-095. $NaNO_2$. j_m, $1/t_s$ vs. E [63Hat]. Parameter: T. j_m: maximum switching current density, t_s: switching time.

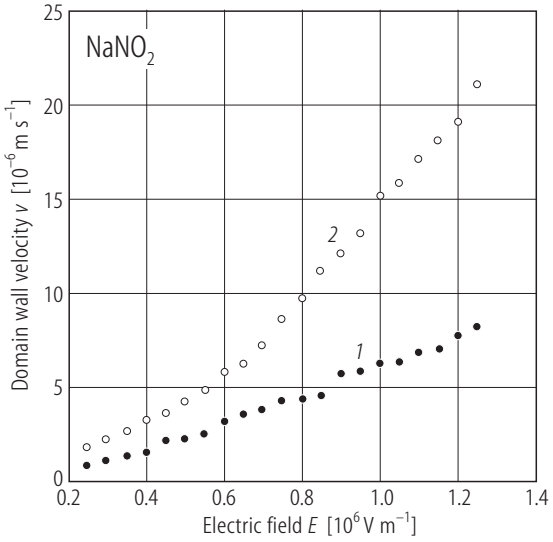

Fig. 28A-1-096. $NaNO_2$. v vs. E [92Mat]. v: domain wall motion velocity. *1*: growing process, *2*: shrinking process.

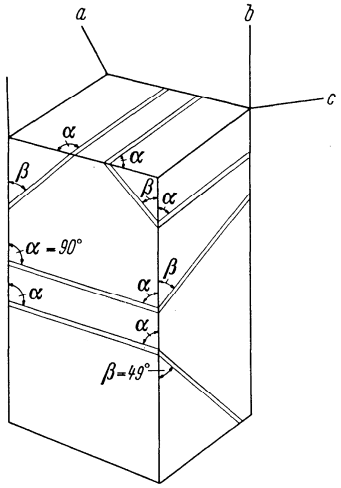

Fig. 28A-1-097. $NaNO_2$. Schematic representation of mechanical twins [63Nak].

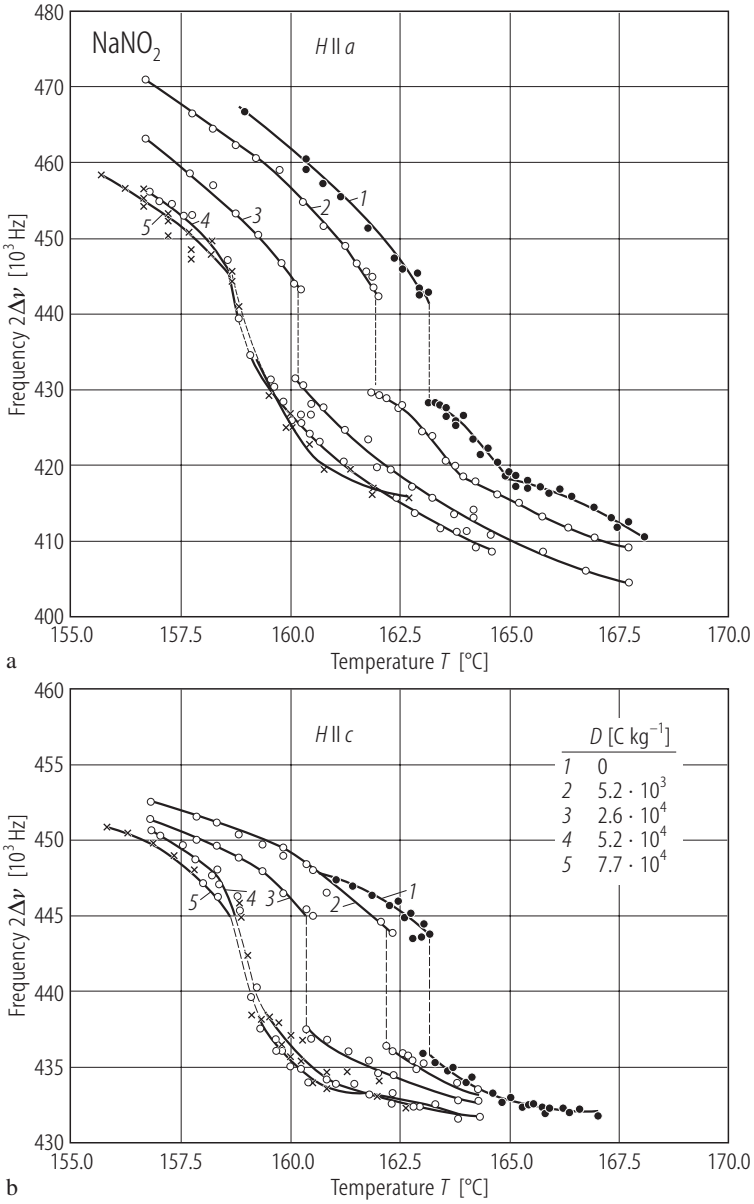

Fig. 28A-1-098. $NaNO_2$. $2\Delta\nu$ vs. T [73Yag]. Parameter: D. $\Delta\nu$: quadrupole splitting of ^{23}Na. D: ^{60}Co γ-ray irradiation dose. (**a**) $\boldsymbol{H} \parallel \boldsymbol{a}$, (**b**) $\boldsymbol{H} \parallel \boldsymbol{c}$.

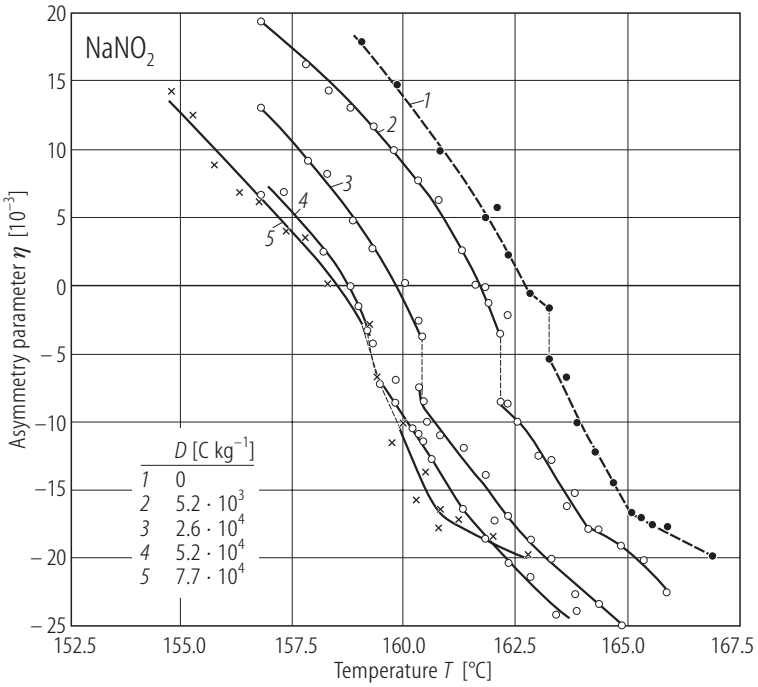

Fig. 28A-1-099. $NaNO_2$. η vs. T [73Yag]. Parameter: D. η: asymmetry parameter. D: ^{60}Co γ-ray irradiation dose.

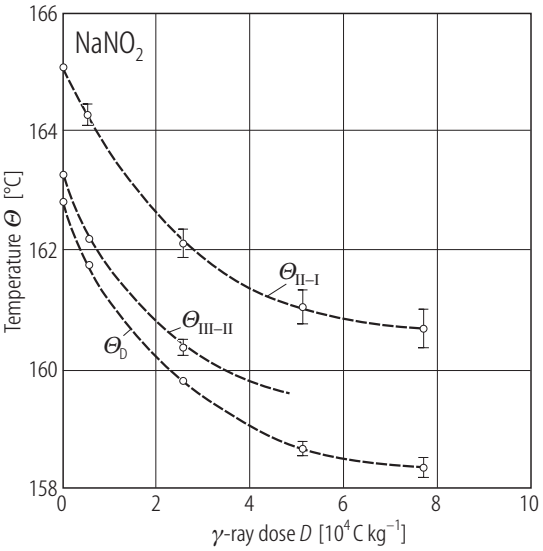

Fig. 28A-1-100. $NaNO_2$. Θ_{II-I}, Θ_{III-II}, Θ_D vs. D [73Yag]. Θ_D: temperature at which asymmtry parameter of ^{23}Na NQR splitting $\eta = 0$. D: ^{60}Co γ-ray irradiation dose.

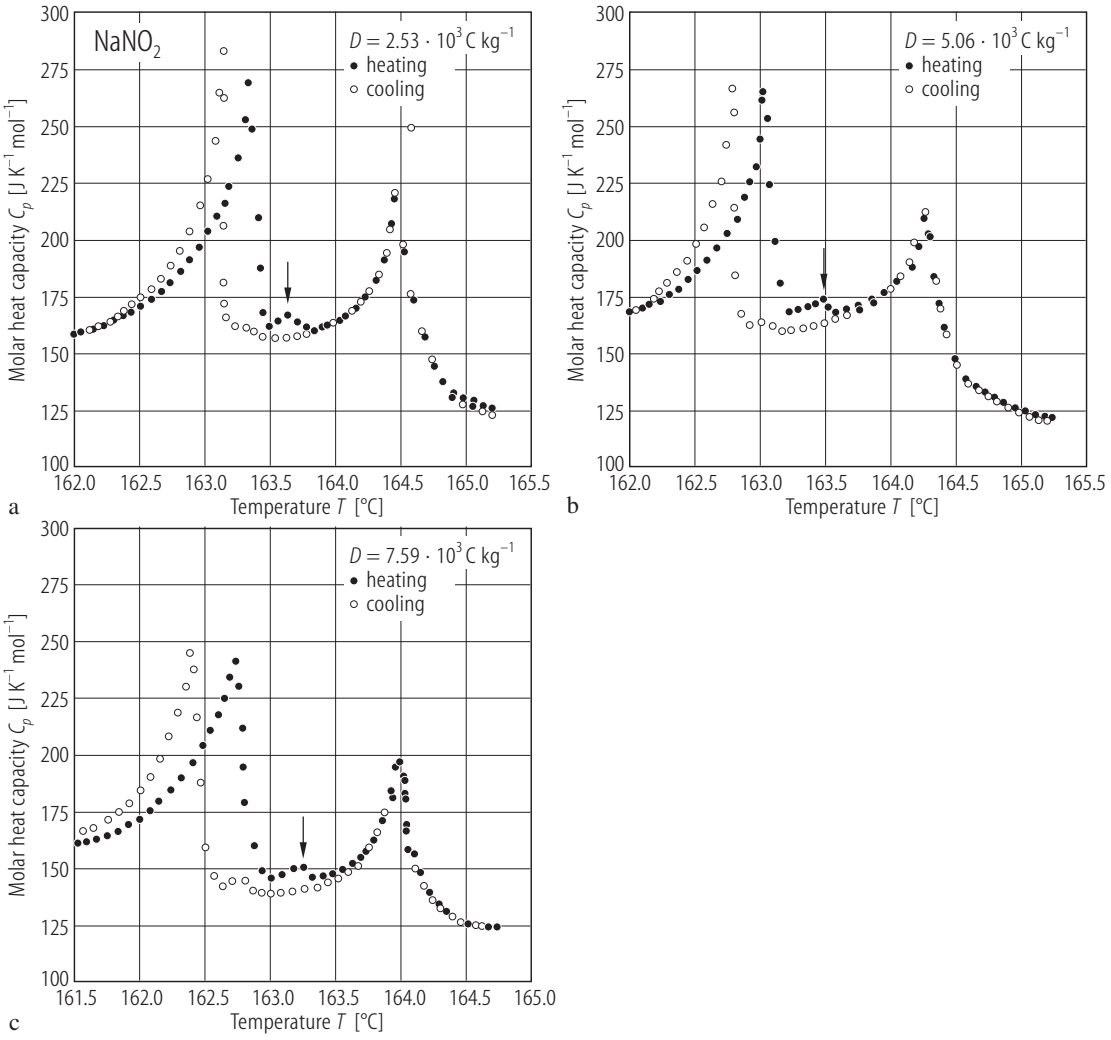

Fig. 28A-1-101. $NaNO_2$. C_p vs. T in the vicinity of the III–II–I transitions [87Yoo]. Parameter: D. D: ^{60}Co γ-ray irradiation dose.

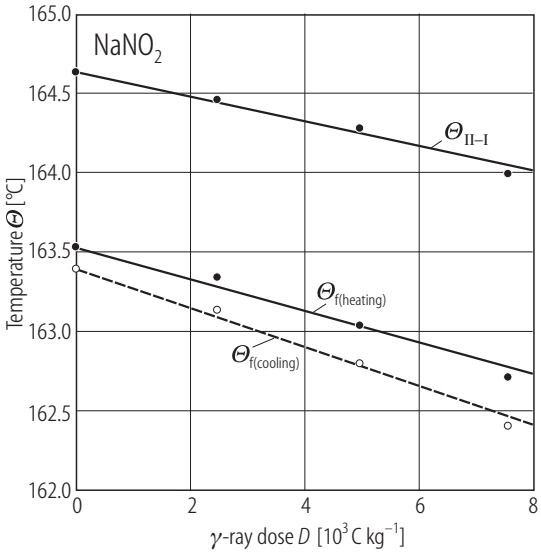

Fig. 28A-1-102. $NaNO_2$. $\Theta_{II–I}$, Θ_f ($=\Theta_{III–II}$) vs. D [73Yag]. D: ^{60}Co γ-ray irradiation dose. Obtained by C_p measurements. See also Fig. 28A-1-100.